HHS Public Access

Author manuscript

Dev Cell. Author manuscript; available in PMC 2019 September 24.

Published in final edited form as:

Dev Cell. 2018 September 24; 46(6): 767–780.e7. doi:10.1016/j.devcel.2018.08.006.

Myomaker and Myomerger work independently to control distinct steps of membrane remodeling during myoblast fusion

Evgenia Leikina[#1], **Dilani G. Gamage**[#2], **Vikram Prasad**[2], **Joanna Goykhberg**[1], **Michael Crowe**[3], **Jiajie Diao**[3], **Michael M. Kozlov**[4], **Leonid V. Chernomordik**[1,*], and **Douglas P. Millay**[2,5,7,*]

[1]Section on Membrane Biology, Eunice Kennedy Shriver NICHD, National Institutes of Health, Bethesda, MD, 20892, USA

[2]Division of Molecular Cardiovascular Biology, Cincinnati Children's Hospital Medical Center, Cincinnati, OH, 45229, USA

[3]Department of Cancer Biology, University of Cincinnati, Cincinnati, OH, 45229, USA

[4]Department of Physiology and Pharmacology, Sackler Faculty of Medicine, Tel Aviv University, Tel Aviv, 69978, Israel

[5]Department of Pediatrics, University of Cincinnati College of Medicine, Cincinnati, OH, 45229, USA

[7]Lead contact

[#] These authors contributed equally to this work.

Summary

Classic mechanisms for membrane fusion involve transmembrane proteins that assemble into complexes and dynamically alter their conformation to bend membranes, leading to mixing of membrane lipids (hemifusion) and fusion pore formation. Myomaker and Myomerger govern myoblast fusion and muscle formation, but are structurally divergent from traditional fusogenic proteins. Here, we show that Myomaker and Myomerger independently mediate distinct steps in the fusion pathway, where Myomaker is involved in membrane hemifusion and Myomerger is necessary for fusion pore formation. Mechanistically, we demonstrate that Myomerger is required on the cell surface where its ectodomains stress membranes. Moreover, we show that Myomerger drives fusion completion in a heterologous system independent of Myomaker, and that a Myomaker-Myomerger physical interaction is not required for function. Collectively, our data

[*]Correspondence: chernoml@mail.nih.gov (L.V.C.), douglas.millay@cchmc.org (D.P.M.).

Author Contributions

E.L., D.G.G., V.K., J.D., L.V.C., and D.P.M. designed experiments. E.L., D.G.G., V.K., J.G., and M.C. performed experiments. E.L., D.G.G., L.V.C., and D.P.M. analyzed the data. M.M.K. contributed to the interpretations of the results. L.V.C. and D.P.M. wrote the manuscript with assistance from all authors.

Declarations of Interests

Douglas P. Millay has filed provisional patents related to this work.

identify a step-wise cell fusion mechanism in myoblasts where different proteins are delegated to perform unique membrane functions essential for membrane coalescence.

Graphical Abstrac

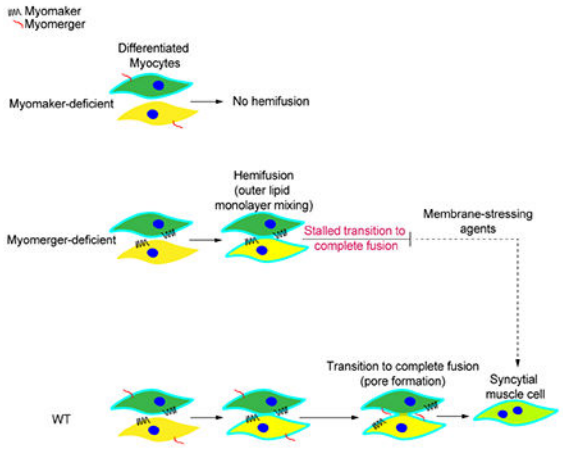

eTOC

An eTOC blurb should also be included that is no longer than 50 words describing the context and significance of the findings for the broader journal readership. When writing this paragraph, please target it to non-specialists by highlighting the major conceptual point of the paper in plain language, without extensive experimental detail. The blurb must be written in the third person and refer to “First Author et al.”

Myoblast fusion is essential for muscle development, regeneration, and growth. Leikina et al. reveal that myoblasts proceed through a fusion mechanism characterized by a division of labor between muscle fusion proteins. The independent and sequential membrane functions of different proteins (Myomaker and Myomerger) culminate in membrane coalescence.

Introduction

Membrane fusion is a multistep process that upon completion unites two membranes and the volumes they surround, and is fundamental for multiple biological processes including exocytosis, viral infection, and development of syncytial tissues (Hernandez and Podbilewicz, 2017). Protein fusion machines facilitate membrane coalescence by overcoming energy barriers through formation of fusion intermediates. The widely accepted mechanism for this is based on interactions between protein(s) anchored in each of the membranes, where the proteins undergo a conformational change that bends the membranes and brings them in close proximity. Examples of this mechanism include SNARE-mediated intracellular vesicle fusion(Jahn and Sudhof, 1999; Weber et al., 1998), virus-cell fusion triggered by influenza hemagglutinin (HA) (Blijleven et al., 2016; Ivanovic and Harrison, 2015; Kielian and Rey, 2006; White et al., 2008), developmental cell fusion of epithelial cells in *C. elegans* driven by Epithelial Fusion Failure-1 (Eff-1) (Perez-Vargas et al., 2014), and HAP2-mediated gamete fusion in alga (Fedry et al., 2017; Valansi et al., 2017). Fusion

intermediates do not necessarily progress to fusion completion as these diverse fusion reactions can stall at intermediate steps including hemifusion, defined as the merger of only contacting monolayers of two membranes, and small fusion pores (Chernomordik and Kozlov, 2003; Cohen and Melikyan, 2004; Podbilewicz et al., 2006; Valansi et al., 2017; Wen et al., 2017; Xu et al., 2005). In contrast, it is difficult to capture fusion intermediates in myoblasts indicating the presence of highly efficient machinery that expands early membrane connections to generate multinucleated myotubes (Leikina et al., 2013). The mechanisms by which myoblasts establish and transition fusion connections are not understood.

A major reason for the lack of mechanistic insight into myoblast fusion has been the difficulty to uncouple the fusion event from pre-fusion processes. Numerous factors, most notably actin-nucleation pathways, regulate myoblast fusion, however it is not known if they regulate the membrane remodeling required for the fusion reaction (Demonbreun et al., 2015; Deng et al., 2017; Duan and Gallagher, 2009; Duan et al., 2012; Gruenbaum-Cohen et al., 2012; Hamoud et al., 2014; Hochreiter-Hufford et al., 2013; Horsley et al., 2003; Nowak et al., 2009; Randrianarison-Huetz et al., 2017; Schejter, 2016b; Schwander et al., 2003; Sens et al., 2010; Vasyutina et al., 2009). We and others discovered two essential muscle-specific myoblast fusion proteins, Myomaker and Myomerger, that together reconstitute fusion in otherwise non-fusing cells suggesting that these proteins catalyze the membrane fusion reaction in myoblasts (Bi et al., 2017; Millay et al., 2013; Quinn et al., 2017; Zhang et al., 2017). Myomaker is a multi-pass membrane protein required on the surface of myoblasts for fusion (Gamage et al., 2017), and mutations of this protein in humans cause a congenital myopathy (Di Gioia et al., 2017). The precise biochemical function for Myomaker is unknown and the structural characteristics include a 221 amino acid protein with seven transmembrane domains, which exhibits little homology to other characterized fusion proteins (Millay et al., 2016). Myomaker is required on both fusing cells, and Myomaker^{+} fibroblasts fuse to myoblasts but do not fuse to each other suggesting that Myomaker activates fusion-competence (Quinn et al., 2017). Myomerger (Quinn et al., 2017), an 84 amino acid protein also referred to as Minion (Zhang et al., 2017) and Myomixer (Bi et al., 2017), induces fusion of Myomaker^{+} fibroblasts and is required in only one of the two fusing cells (Quinn et al., 2017; Zhang et al., 2017). Myomerger, like Myomaker, harbors little homology to classical fusogens, although there are some similarities with fusion associated small transmembrane (FAST) proteins of several non-enveloped viruses, which utilize cell-cell fusion to spread the infection (Ciechonska and Duncan, 2014). While it is clear that Myomaker and Myomerger are necessary and sufficient for cellular fusion, how these two factors that are strikingly different from the best characterized fusion proteins cooperate to drive membrane coalescence is unknown.

Membrane fusion is typically achieved by one protein or protein complex that work together to elicit each of the membrane remodeling effects to achieve hemifusion and pore formation. Here we show that myoblasts proceed through a novel step-wise fusion reaction, where Myomaker and Myomerger govern different stages of the fusion pathway to form multinucleated skeletal muscle. We demonstrate that a physical interaction between Myomaker and Myomerger is not required for their individual activities and that Myomaker

controls formation of early fusion intermediates and Myomerger drives the transition beyond these intermediates to fusion completion.

Results

Myomaker and Myomerger govern distinct aspects of the fusion pathway

To decipher mechanisms of myoblast fusion, we probed the precise stage of fusion that is arrested in myoblasts lacking either Myomaker or Myomerger. We utilized an assay that distinguishes hemifusion, detected as lipid mixing in the absence of content mixing, from fusion pore formation and expansion at the later stages of fusion, detected as content mixing and syncytium formation, respectively. We differentiated C2C12 myoblasts and labelled one population with both a lipid probe (DiI) and a content probe (green cell tracker), then this population was mixed with unlabeled cells and incubated for 24 hours (Figure 1A). Due to continuous membrane trafficking in living cells, by the time fusion is evaluated many hours after cell labeling, fluorescent lipids are already distributed between the plasma membrane and intracellular membrane compartments. Multinucleated cells with both lipid and content probes indicate complete fusion. The cells that formed hemifusion connections but did not advance to complete fusion were identified as mononucleated cells containing the lipid probe but not the content probe. Note that lipid probe redistribution between the cells in the absence of content mixing is strong evidence for hemifusion, since fusion pores that would allow cell-to-cell passage of labeled intracellular vesicles would even more so allow passage of much smaller content probes. In WT cultures we observed mainly multinucleated cells (complete fusion) and a small number of hemifusion events (Figure 1B), which was expected because WT cells are primed to drive early fusion intermediates to full fusion (Leikina et al., 2013). While we observed minimal hemifusion events in Myomaker$^{-/-}$ C2C12 cultures, hemifusion was readily detected in Myomerger$^{-/-}$ C2C12 cells (Figure 1B). Quantification of hemifusion and complete fusion revealed a significant reduction of hemifusion in Myomaker$^{-/-}$ myoblasts, but an accumulation of hemifused Myomerger$^{-/-}$ cells (Figure 1C). Complete fusion was reduced in both cell types (Figure 1C). Thus, Myomerger-deficient C2C12 myoblasts stall at an early intermediate stage as the fusion reaction cannot progress beyond the hemifusion step. The conclusion that fusion between Myomerger$^{-/-}$ cells is blocked downstream of hemifusion was confirmed with a different cell labeling strategy. Incubation of Myomerger$^{-/-}$ differentiated C2C12 myoblasts labeled with either membrane probe DiI or membrane probe DiO yielded mononucleated cells labeled with both probes for Myomerger$^{-/-}$ myoblasts but almost no such cells for WT and Myomaker$^{-/-}$ myoblasts (Figure S1A). Similar experiments on primary myoblasts from Myomaker$^{-/-}$ and Myomerger$^{-/-}$ mice confirmed that Myomaker deficiency blocks lipid mixing and Myomerger deficiency arrests fusion downstream of lipid mixing (Figure S1B).

The cell labeling strategies above do not detect fusion pores that do not expand to allow syncytial formation. To test if Myomerger$^{-/-}$ myoblasts can form small pores, we co-plated differentiated Myomerger$^{-/-}$ C2C12 myoblasts labeled with either green cell tracker or orange cell tracker (Figure 1D). We observed double-labeled cells in WT, but not in Myomerger$^{-/-}$ cultures, indicating that Myomerger-deficient cells do not form fusion pores large enough to allow redistribution of the cell trackers (Figure 1E and Figure 1F). Taken

together, these data indicate that Myomaker and Myomerger govern distinct steps of the membrane fusion reaction in myoblasts, where Myomaker functions at or upstream of hemifusion and Myomerger drives pore formation.

Myomaker activity does not require Myomerger

To probe the mechanisms underlying the involvement of Myomerger in pore formation, we developed multiple strategies to functionally compensate for Myomerger deficiency. In our first approach, we subjected the cells to hypotonic osmotic shock. Cell swelling generates tension and stress on the membrane lipid bilayer, and is a well-known method to force cell fusion completion if hemifusion connections are already present (Chernomordik et al., 1998; Melikyan et al., 1995). We differentiated WT, Myomaker$^{-/-}$, and Myomerger$^{-/-}$ myoblasts for 48 hours, labeled them with lipid and content probes and co-plated the labeled cells with unlabeled cells for 24 hours in differentiation medium to allow establishment of hemifusion connections. Then the cells were treated with a hypotonic buffer (1:3 PBS:Water) for 60 seconds (Figure 2A). Hypotonic shock had no detectable effect on myotube formation in WT cultures confirming that all hemifusion events in these cells advanced to complete fusion. Myomaker$^{-/-}$ cells did not respond to hypotonic shock confirming the lack of hemifusion connections in Myomaker-deficient myoblasts (Figure 2B). In contrast, complete fusion was observed in Myomerger$^{-/-}$ cells after hypotonic shock further indicating that hemifusion connections are present in these cells (Figure 2B and Figure 2C). Similarly, hypotonic shock induced fusion of Myomerger null primary myoblasts (Figure S2A).

Since the mechanism by which hypotonic shock resolves hemifusion connections is through global membrane bilayer stress, we also tested if more subtle modifications of membrane bilayer could drive fusion. We found that fusion of Myomerger-deficient myoblasts can be rescued by the detergent Octyl-α-Glucoside (OG) and by the anti-microbial peptide Magainin 2 (Mag2), both known to directly interact with the lipid bilayer and generate membrane stresses that cause permeabilization (Matsuzaki et al., 1998; Nazari et al., 2012; Patel et al., 2014). We applied OG to differentiated Myomaker$^{-/-}$ and Myomerger$^{-/-}$ myoblasts for 30 minutes and then washed the cells. Fusion was assessed 5 hours after the treatment. We found that Myomaker$^{-/-}$ cells treated with OG did not fuse, but we observed obvious fusion events in Myomerger$^{-/-}$ cells (Figure 2D). The ability of OG to compensate for loss of Myomerger was confirmed in primary myoblasts (Figure S2B). Application of Mag2 also partially rescued fusion of Myomerger$^{-/-}$ myoblasts. Fusion was increased in Myomerger$^{-/-}$, but not Myomaker$^{-/-}$, myoblasts after 20 hours of incubation with Mag2 (Figure 2E). The ability of OG and Mag2 to increase fusion was quantified by analyzing the percentage of myosin^{+} (a marker of muscle differentiation) cells with 3 or ≥ 4 nuclei. OG and Mag2 not only increased the percentage of cells with 3 nuclei but also induced formation of myotubes with ≥ 4 nuclei (Figure 2F). OG or Mag2 did not have an effect on fusion of WT C2C12 myoblasts (Figure S2C and S2D), revealing that WT cells are maximally efficient at converting hemifusion to full fusion thus the reaction does not stall at intermediate stages.

The extent of fusion rescue for Myomerger$^{-/-}$ myoblasts above, while significant, did not reach WT levels. We hypothesized that the magnitude of rescue could be limited by the

transient character of hemifusion intermediates. Myoblast fusion is a relatively slow process where many multinucleated myotubes form over multiple days. Thus, at any given time there are a finite number of hemifusion connections. These connections are energy intensive structures that, if not converted into complete fusion, dissociate within minutes (Chernomordik and Kozlov, 2003; Leikina and Chernomordik, 2000). We reasoned that the treatments promoting hemifusion-to-fusion transition for the myomerger-deficient myoblasts will be more effective if applied to cells undergoing synchronized fusion. WT, Myomaker $^{-/-}$, or Myomerger$^{-/-}$ C2C12 myoblasts, labeled with either green cell tracker or orange cell tracker, were differentiated for 48 hours and then the reversible hemifusion inhibitor lysophosphatidylcholine (LPC) was applied for 16 hours in differentiation medium (Leikina et al., 2013) (Figure 3A). At the time of LPC removal, we treated the cells with either hypotonic medium (1:3 PBS:H_2O) or chlorpromazine (CPZ) (Chernomordik and Kozlov, 2003; Leikina and Chernomordik, 2000; Melikyan et al., 1997), which is also known to induce hemifusion-to-fusion transition, for 60 seconds. The percentage of nuclei in multinucleated cells was assayed as syncytium formation 30 minutes after LPC removal. We compared these treatments to uninterrupted fusion where myoblasts were not exposed to LPC (Control (-LPC)) (Figure 3A). Application of either hypotonic shock or CPZ had little effect on fusion of WT myoblasts (Figures 3B and 3C). This indicates that hemifusion intermediates in WT cells effectively advance to complete fusion without further treatments, reinforcing the absence of stalled intermediates in WT cells. No fusion was observed for Myomaker$^{-/-}$ cells in the absence of LPC or after treatment the LPC-synchronized cells with hypotonic shock or CPZ, confirming that these cells do not hemifuse (Figures 3B and 3C). Finally, synchronized Myomerger$^{-/-}$ myoblasts subjected to either hypotonic shock or CPZ reached fusion levels observed for WT myoblasts (Figure 3C). A robust rescue of fusion in these experiments by treatments promoting hemifusion-to-fusion transition demonstrates that the lack of Myomerger does not impact the efficiency of hemifusion and that Myomaker does not require Myomerger to establish hemifusion connections capable of being transitioned to full fusion. Moreover, pleiotropic membrane stresses that promote pore formation can compensate for loss of Myomerger.

Myomerger contains a C-terminal ectodomain that functions from outside the cell.

We next sought to understand the mechanisms by which Myomerger drives fusion completion. Myomerger contains three conserved α-helical domains that could presumably interact with a membrane, and the second helix is highly conserved suggesting an important function (Shi et al., 2017). However, whether Myomerger is an integral membrane protein, its positioning in or at the plasma membrane, and the cellular location for its function are not known. In contrast to the downstream helical domains (amino acids 29-40 and 43-57), the N-terminal α-helix of Myomerger (amino acids 5-25) is long enough to span the bilayer (Figure S3A). To test if Myomerger is an integral membrane protein we fractionated membranes from WT C2C12 myoblasts on day 2 of differentiation. Membrane fractions were then incubated with either low salt buffer, high salt buffer (1M NaCl), alkaline buffer (pH 11), or detergent (1% SDS), followed by centrifugation and assessment of membrane and soluble fractions by western blot. While high salt and alkaline buffers solubilized the peripheral membrane protein Golgin 97, Myomerger remained with the pelleted membrane fraction (Figure S3B). Myomerger was only solubilized with detergent indicating that this

protein is tightly associated with the membrane. To confirm the N-terminal region is not a signal sequence cleaved during protein processing, we expressed a full-length Myomerger (rMyomerger$^{1-84}$) protein and a Myomerger protein lacking the N-terminal region (rMyomerger$^{26-84}$) in *E. coli* (Figure S3C). Comparison of these proteins to WT C2C12 lysates by western blotting for Myomerger revealed that endogenous Myomerger migrates at a size similar to rMyomerger$^{1-84}$, whereas rMyomerger$^{26-84}$ runs at a lower molecular weight (Figure S3D).

To assess the functional importance of the N-terminal helical region we generated a mutant where amino acids 5-25 of Myomerger were replaced with a cleavable synthetic signal sequence from HA (Guan et al., 1992; Millay et al., 2016). We expressed this mutant (Myomerger$^{\Delta 1-25}$) or WT Myomerger in Myomerger$^{-/-}$ myoblasts. While WT Myomerger and Myomerger$^{\Delta 1-25}$ were expressed at similar levels (Figure S3E), only WT Myomerger was able to rescue fusion (Figure S3F). Isolation of membrane fractions showed that Myomerger$^{\Delta 1-25}$ also associated with membranes (Figure S3G), indicating that the N-terminal region of Myomerger is not absolutely required for membrane attachment but could be important for orientation of the protein in the membrane or localization to the proper domain. These data establish that the N-terminal α-helical region of Myomerger is required for function when endogenously expressed.

A strong association between membranes and Myomerger leads to the question of which cellular membrane compartment contains this protein. If the protein functions in membrane events that drive fusion it would be expected to be present on the plasma membrane, however whether endogenously expressed Myomerger is localized on the plasma membrane is not known. We labeled proteins at the surface of WT C2C12 cells with a cell-impermeable biotinylation reagent and then immunoprecipitated biotinylated proteins with streptavidin. Immunoblotting of the isolated proteins with Myomerger antibodies showed that Myomerger is normally expressed on the cell surface and suggested that the non-transmembrane region of Myomerger is extracellular (Figure 4A).

To verify that Myomerger-membrane interactions promote fusion rather than some prefusion stages, we employed the synchronized fusion assay described above (Gamage et al., 2017; Leikina et al., 2013). We labeled one population of WT C2C12 myoblasts with a lipid probe (DiI) and the other with a content probe (green cell tracker) and accumulated ready-to-fuse C2C12 cells in the presence of LPC. 30 minutes after replacing LPC-supplemented differentiation medium with normal differentiation medium (LPC/Wash) we measured fusion by the syncytium formation assay and hemifusion by the lipid mixing assay that assesses the appearance of mononucleated double-labeled cells (Figure 4B). Myomerger or non-specific control IgG antibodies were applied at the time of LPC removal. As expected (Leikina et al., 2013), LPC removal (LPC/Wash) resulted in a significant increase in complete fusion relative to that observed in the control experiment in which LPC was not removed (LPC) (Figure 4C). Removal of LPC did not increase the numbers of hemifused cells beyond the background level observed in the presence of LPC reflecting high efficiency of hemifusion-to-fusion transition for WT myoblasts. Control non-specific IgG applied at the time of LPC removal had a minor effect on hemifusion but no impact on complete fusion (Figure 4C). We interpret the minor effect on hemifusion to be due to non-specific binding

of IgG antibodies, which could sterically hinder hemifusion. In contrast to control IgG, application of Myomerger antibodies that recognize the region of the protein after amino acid 25, reduced the number of complete fusion events (Figure 4C). These antibodies also increased the number of cells scored as hemifused at 30 minutes after LPC removal but, possibly, advancing to complete fusion at later time. The synchronized fusion assay on WT primary myoblasts with Myomerger antibodies also revealed an increase in the number of hemifused cells and decrease in the number of complete fusion events in the presence of Myomerger antibodies, confirming a prominent role for cell surface Myomerger in fusion pore formation (Figure S4A and Figure S4B).

Taken together, our data suggest a topology model for Myomerger where the N-terminal helical region is embedded in the plasma membrane and the short helical regions are extracellular (Figure S4C). That the N-terminal mutant (Myomerger$^{\Delta 1\text{-}25}$) tracks with membrane fractions (Figure S3G) suggests that the short extracellular helical regions may interact with the outer layer of the plasma membrane. To explore this model further, we purified the ectodomain of Myomerger and tested its ability to rescue fusion of Myomerger null myoblasts. We expressed in *E. coli* the extracellular region of Myomerger (amino acids 26-84 of the mouse protein) linked to maltose binding protein (MBP) to improve solubility (Nguyen et al., 2017). MBP or MBP- Myomerger$^{26\text{-}84}$ were purified to 95% homogeneity through an amylose column and size exclusion chromatography (Figure S5A). We applied rMBP-Myomerger$^{26\text{-}84}$ or rMBP as a control to either Myomaker$^{-/-}$ or Myomerger$^{-/-}$ myoblasts for 20 hours on day 3 of differentiation, then assessed fusion. rMBP-Myomerger$^{26\text{-}84}$ had no effect on Myomaker$^{-/-}$ C2C12 myoblasts but promoted fusion of Myomerger$^{-/-}$ myoblasts indicating that myoblast fusion depends on the interactions between the ectodomain of Myomerger and the plasma membrane of the myoblasts (Figure 4D). We performed this experiment with multiple concentrations of rMBP or rMBP-Myomerger$^{26\text{-}84}$ and found that Myomerger ectodomains induce formation of myotubes with 4 or more nuclei (Figure 4E). These data are consistent with the model that the ectodomain of Myomerger functions from outside the cell to drive completion of the fusion reaction.

Myomerger functions to stress membranes

Pleiotropic membrane manipulations that we found to compensate for Myomerger deficiency are known to generate membrane stresses leading to pore formation. To test if Myomerger function in fusion involves direct effects of the protein on the membrane lipid bilayer, we first tested if Myomerger directly interacts with lipid bilayers and promotes bilayer permeabilization. We incubated recombinant Myomerger ectodomains with protein-free liposomes encapsulated with sulforhodamine B at self-quenching concentrations. Protein-induced leakage of liposome content dilutes the probe and increases its fluorescence (Figure 5A). Fluorescence was normalized to the fluorescence detected when all liposomes were lysed by application of SDS. Liposome leakage was observed upon addition of rMBP-Myomerger$^{26\text{-}84}$ but not rMBP (Figure 5B). Quantification of liposome leakage two minutes after the addition of various concentrations of protein confirmed an ability for rMBP-Myomerger$^{26\text{-}84}$ to rearrange membrane lipids (Figure 5C). To control for the possibility that the MBP epitope tag impacted our analysis, we removed MBP and purified recombinant

Myomerger$^{26\text{-}84}$ (Figure S5B). rMyomerger$^{26\text{-}84}$ induced liposome leakage (Figure S5C) and rescued synchronized fusion of Myomerger$^{-/-}$ myoblasts (Figure S5D). These findings indicate that the membrane-destabilizing and fusion-rescuing activities of rMBP-Myomerger$^{26\text{-}84}$ do not depend on the MBP tag.

Proteins and peptides can lyse liposomes through multiple mechanisms including directly promoting pore formation in the liposomal bilayer (Chernomordik and Kozlov, 2003; Matsuzaki et al., 1998), by driving liposome-liposome adhesion strong enough to deform and rupture the liposomes (Rand et al., 1985), or by inducing liposome fusion that in some cases may be accompanied by a temporal increase in bilayer permeability ("leaky fusion") (Yang et al., 2010). To assess if Myomerger induces liposome leakage through an adhesion-dependent mechanism, we included 2 mole % of polyethylene glycol (PEG-PE) 2000 grafted lipid into the liposome composition. While these and even lower amounts of PEGylated lipid strongly suppress liposome aggregation (Cummings and Vanderlick, 2007), rMyomerger$^{26\text{-}84}$ effectively permeabilized PEGylated liposomes indicating that it does so through an adhesion-independent mechanism (Figure S5E). Next, to determine if Myomerger-induced liposome leakage is accompanied by lipid mixing we incubated DiI- and DiD-labeled liposomes with unlabeled liposomes, and then added rMyomerger$^{26\text{-}84}$. In this FRET-based system, where DiI is the donor and DiD is the acceptor, lipid mixing between labeled and unlabeled liposomes would dilute the FRET between DiI and DiD and result in an increase of DiI emission. At the end of each of the FRET experiments, we added detergent to measure DiI emission corresponding to infinite dilution of the probes (100% lipid mixing). While 1.25 μM (1 protein per 40 lipids) and higher concentrations of rMyomerger$^{26\text{-}84}$ induced lipid mixing (Figure S5F), lower concentrations of the protein that we found to be sufficient to induce leakage (Figure S5C), did not induce lipid mixing indicating that liposome leakage does not depend on fusion. This conclusion was further substantiated by finding that supplementing liposome composition with PEGylated lipid suppresses lipid mixing but not liposome leakage (Figure S5F,E). The finding that liposome leakage does not depend on either adhesion or fusion of the liposomes indicates a direct lipid-destabilizing activity for the ectodomain helices of Myomerger.

In another approach, to explore whether Myomerger expression alters cell membrane properties that are important for pore formation, we focused on the ability of myoblasts to withstand hypotonic osmotic shock. Exposure to distilled water increases osmotic pressure across the plasma membrane, removes excess surface area and generates tension in the plasma membrane (Finkelstein et al., 1986; Pietuch et al., 2013). When the critical membrane tension is reached, it generates pore(s) resulting in a membrane that is now permeable to normally impermeable molecules. The higher propensity for the membrane lipid bilayer to form a pore, the lower the critical tension required for permeabilization of plasma membrane of the cells subjected to the osmotic shock. We examined the effects of Myomaker and Myomerger expression on the osmotic shock-induced permeabilization of C2C12 cells. The cells were incubated in water for 30 seconds in the presence of a fluorescent F-actin probe (phalloidin) that does not enter intact cells. Cells with the pores were identified as being phalloidin^{+} (Figure 5D). Correlation of Myomerger expression with elevated sensitivity to osmotic shock was illuminated by the finding that proliferating WT C2C12 myoblasts that do not express Myomerger were less sensitive to osmotic shock (i.e. a

lower percentage of the cells became phalloidin^{+} after application of hypotonic osmotic shock) compared to differentiating WT C2C12 cells (Figure 5E). Moreover, we observed that differentiating Myomerger$^{-/-}$ myoblasts were less sensitive to osmotic shock than WT and Myomaker$^{-/-}$ myoblasts, as evidenced by a lower percentage of permeabilized Myomerger$^{-/-}$ cells (Figure 5E and Figure 5F). Each of these findings are consistent with the idea that Myomerger facilitates pore formation in the lipid bilayer of the plasma membranes of differentiating myoblasts.

Myomerger drives fusion completion independent of myomaker

Our data thus far indicate that Myomaker and Myomerger govern distinct aspects of the fusion reaction and suggest a step-wise fusion reaction in myoblasts, where different proteins perform independent functions that culminate in membrane coalescence. Further support for this model is that Myomaker can establish hemifusion connections in the absence of Myomerger (Figure 3). If the reaction proceeds through a step-wise mechanism with independent functions one would predict that a physical interaction between Myomaker and Myomerger is not obligatory for function. Thus, we next sought to determine if Myomerger possesses an activity independent of Myomaker and probed the requirement for a physical interaction.

A physical interaction was previously demonstrated between FLAG-Myomaker and Myomerger through co-immunoprecipitations (co-IP) after acute retroviral infection (Bi et al., 2017), leading to the idea that an interaction was important for function. While we have confirmed a physical interaction between FLAG-Myomaker and Myomerger in the acute retroviral system (Figure S6A), we have not detected co-localization in intracellular compartments in differentiated myoblasts using standard confocal microscopy (Quinn et al., 2017). We also did not detect a physical interaction in C2C12 myoblasts overexpressing untagged Myomaker with endogenous levels of Myomerger (Figure S6B), and found no co-localization of these proteins through super-resolution microscopy (Figure S6C). Moreover, an independent group has also not observed any interaction (Zhang et al., 2017), thus whether Myomaker and Myomerger directly interact and work as a complex remains an open question.

One complication with the detected physical interaction is that it is achieved through retroviral infection, which requires the presence of a viral fusogen that could impact the reconstitution assay. We thus established an inducible fusion reconstitution system that does not rely on acute retroviral infection. 10T½ fibroblasts were transduced sequentially with a Myomaker retrovirus and a lentivirus containing a Dox-inducible Myomerger construct, then selected with puromycin over multiple passages. Myomaker was expressed in −Dox and +Dox samples but Myomerger expression was only detected after the addition of Dox (Figure S6D). A Myomaker-Myomerger interaction by co-IP was not detected using the same detergent conditions as in the retroviral system, however fusion was reconstituted (Figure S6E and Figure S6F). We also generated two additional cell lines with FLAG-tagged proteins. No physical interaction was detected in Myomaker^{+} fibroblasts with Dox-inducible Myomerger-FLAG despite an induction of fusion (Figure S6G and Figure S6H). FLAG-Myomaker^{+} fibroblasts with Dox-inducible Myomerger also did not yield a physical

interaction and fusion was not reconstituted (Figure S6I and Figure S6J). This suggests that FLAG-Myomaker does not fully recapitulate untagged Myomaker function, which is consistent with previous observations (Gamage et al., 2017; Millay et al., 2016), and raises the possibility that the interaction detected in acute retroviral systems may not be functionally relevant. Our data indicate that Myomaker and Myomerger collaboration in fusion does not require a physical interaction between these proteins.

The absence of detectable Myomaker-Myomerger complexes supports our hypothesis that these proteins have independent and distinct functions. While Myomaker and Myomerger may form transient interactions that are difficult to capture, a more important question is whether Myomerger drives fusion completion in the absence of Myomaker. We used a heterologous fusion assay between 3T3 fibroblasts, expressing the viral fusogen hemagglutinin (HA), and erythrocytes (red blood cells, RBCs) containing both lipid and content probes (Figure 6A). We transfected HA-expressing fibroblasts with either empty vector, Myomaker, or Myomerger, and mixed the cells with labeled RBCs. We confirmed expression of Myomaker and Myomerger in fibroblasts through immunostaining (Figure S7). HA binding to sialic acid receptors at the surface of RBCs brings the membranes of HA^+ fibroblasts and RBCs into very tight contact (Leikina et al., 2004). To acquire fusion-competence, HA has to be first cleaved by trypsin and then activated by acidic pH. Lowering the number of fusion-competent HAs in HA^+ fibroblasts by using reduced trypsin concentrations and suboptimal pH decreases fusion extents, and shifts the observed fusion phenotype from full fusion (lipid- and content-mixing) to mostly hemifusion (lipid mixing without content mixing) (Figure 6A) (Chernomordik et al., 1998). Under these conditions, more hemifusion events (since fibroblasts are much larger than RBCs, hemifusion events are seen as appearance of large cells labeled with only lipid probe) compared to fully fused cells (fibroblasts with content probe) were observed in empty and $Myomaker^+$ HA^+ fibroblasts (Figure 6B). In contrast, complete fusion events were readily observed in Myomerger-expressing HA^+ fibroblasts (Figure 6B). Quantification of hemifusion and complete fusion as a percentage of RBCs that transferred to fibroblasts only lipid probe (hemifusion) or both lipid and content probe (complete fusion) shows a significant increase in complete fusion when HA^+ fibroblasts are expressing Myomerger (Figure 6C). This finding demonstrates that Myomerger drives fusion pore formation and fusion completion in a Myomaker-independent manner.

Discussion

Myoblast fusion is fundamental for proper muscle development and regeneration (Millay et al., 2013; Millay et al., 2014; Sampath et al., 2018), and dysregulation of the process leads to myopathies (Di Gioia et al., 2017). In this report, we further the understanding of myoblast fusion by demonstrating that this fusion reaction proceeds through a novel step-wise mechanism where different proteins function at independent points in the pathway. We propose a model in Figure 7 where Myomaker function is essential for fusion initiation and formation of hemifusion intermediates, and Myomerger drives subsequent fusion pore formation and expansion by generating membrane stresses. In more well-characterized fusion systems (viral and intracellular membrane fusion), reactions can be stalled at the hemifusion stage, but both hemifusion and pore formation are driven by the same protein

complex (Podbilewicz, 2014). Thus, we have revealed a membrane fusion mechanism that is divergent from well-established models of fusion such as SNARE-mediated intracellular fusion, HA-mediated viral fusion, and Eff-1 developmental fusion.

The discovery of two essential factors for myoblast fusion has led to questions about how they may work together to drive the process. Tentative models propose that Myomerger binds to and activates Myomaker or that Myomaker positions Myomerger and other fusion factors in proper membrane domains (Bi et al., 2018; Bi et al., 2017; Shi et al., 2017). Our data indicate that Myomaker does not need Myomerger to mediate hemifusion. Indeed, the treatments promoting hemifusion-to-fusion transition of Myomerger$^{-/-}$ myoblasts result in levels of complete fusion comparable to WT levels, showing that the lack of Myomerger does not compromise Myomaker-dependent hemifusion. Similarly, we also establish that Myomerger has no obligate requirement for Myomaker to complete the fusion reaction. Myomerger can drive completion of heterologous fusion reactions mediated by the viral fusion protein HA, a system completely devoid of Myomaker. Furthermore, we utilized extensive co-IP analysis and super-resolution microscopy to demonstrate a lack of physical interaction, or obvious colocalization, between Myomaker and Myomerger. We only detect a physical interaction with epitope-tagged versions of Myomaker after retroviral infection, which has previously been reported. While our analysis does not preclude the possibility that Myomaker and Myomerger interact in discrete domains on the plasma membrane, or an interaction could be detected with certain detergents or improved antibodies, our results suggest that physical interactions between these proteins are irrelevant for their function in myoblast fusion.

Our data indicate that myoblast fusion stalls at hemifusion in the absence of Myomerger. Indeed, cell-to-cell redistribution of lipid probe in the absence of redistribution of content probe is a defining hallmark of hemifusion. The conclusion that Myomerger-deficient cells form hemifusion connections was further supported by two independent experimental approaches that do not utilize lipid mixing assay. We found that fusion intermediates formed by Myomerger-deficient cells could be effectively transformed into full fusion by mild hypotonic shock and CPZ applications, two treatments used in studies on viral fusion to reveal hemifusion structures by their transformation into full fusion (Leikina and Chernomordik, 2000; Melikyan et al., 1997). Since neither of the three hemifusion-revealing approaches we used (lipid mixing assay, hypotonic shock and CPZ applications), detected hemifusion for Myomaker-deficient cells, we conclude that Myomaker functions at the hemifusion stage or prior to it. The details for how Myomaker mediates hemifusion remain to be elucidated. Key questions here include whether Myomaker directly controls hemifusion, potentially by acting in *trans* on both fusing cells to bring membranes in close enough proximity to mix lipids, or indirectly through cooperation with additional cellular machinery. The stalling of fusion at the hemifusion stage in Myomerger$^{-/-}$ myoblasts provides the first evidence of a ‘divided’ fusion reaction. Since other developmental cell-cell fusion processes apparently also proceed through hemifusion intermediates (Podbilewicz et al., 2006; Valansi et al., 2017; Verma et al., 2014), some or all of these processes may utilize a similar division of functions between fusogenic proteins providing a regulatory checkpoint to ensure fidelity of the fusion reaction.

Myomerger possesses membrane stressing activities potentially through its helical regions in the ectodomain. The first helical region in the ectodomain has an amphipathic character and is 12 amino acids, whereas the second helix is strictly hydrophobic and contains 15 amino acids. Precise mechanisms by which these helical regions in the ectodomain induce membrane destabilization will be the focus of future investigations. It has been suggested that Myomerger may induce fusion through control of actin cytoskeletal organization as chemical disruption of actin dynamics inhibits fusion mediated by Myomaker and Myomerger (Zhang et al., 2017). This function for Myomerger would be more likely if it worked from inside the cell. However, previous work showed that Myomerger containing a C-terminal FLAG tag was detectable by live staining (Bi et al., 2018), suggesting extracellular localization of the non-transmembrane region of Myomerger. Our surface biotinylation experiments in which we found lysines in the C-terminal region of Myomerger (the only lysines in the protein) to be biotinylated by a membrane impermeable reagent substantiated this conclusion. Furthermore, antibodies to the Myomerger ectodomain inhibit synchronized fusion showing functional importance of Myomerger ectodomain located at the surface of myoblasts. However, we can not exclude a scenario in which Myomerger influences actin dynamics acting from outside the cell (Beck et al., 2001). The role of the actin cytoskeleton during myoblast fusion is clearly established (Schejter, 2016; Shilagardi et al., 2013), but it is premature to place Myomaker and Myomerger functions upstream or downstream of the actin rearrangements associated with the cell fusion process. In this study we did not investigate whether Myomerger directly regulates actin dynamics, mainly because at the cellular level it leads to complex interpretations as any observed changes in actin could be a direct result of Myomerger activity or a secondary consequence of its fusogenic role. The ability of Myomerger to directly regulate actin will be best ascertained through biochemical reconstitution assays.

As reported above, Myomerger renders membranes susceptible to permeabilization, and reagents found to compensate for Myomerger deficiency are also known to promote membrane permeabilization. How a protein with this type of activity could drive transition of hemifusion intermediates to fusion completion is not obvious. The most probable site for opening of a fusion pore in the hemifusion intermediate is the stressed three-way junction of concave-shaped (negative curvature) lipid monolayers that come together at the rim of the intermediate (Chernomordik and Kozlov, 2003; Muller and Schick, 2011). Given that Myomerger facilitates opening of pores in a membrane bilayer and thus likely generates convex (positive) curvature of the lipid monolayer (Chernomordik and Kozlov, 2003; Matsuzaki et al., 1998), one possibility is this positive curvature effect of Myomerger at the negatively-curved rim of the hemifusion structure generates additional elastic stresses that nucleates fusion pore formation. Further analysis will be required to understand the exact biophysical mechanisms by which interactions between Myomerger ectodomains and the plasma membrane lipid bilayer promote opening and expansion of a fusion pore.

In summary, we have revealed a novel membrane fusion mechanism where at least two factors divide their fusogenic activities to initiate and drive membrane coalescence and muscle formation. The lack of a required physical interaction between Myomaker and Myomerger, and their functional independence, reveals that the function served by single fusogens in other systems has been separated and assigned to two independently-acting

muscle-specific proteins that function to drive distinct fusion stages. This division of the fusion reaction may afford myocytes with critical regulatory checkpoints that ensure fusion of proper cells types during development and regeneration. It will be interesting if a similar strategy is also utilized by other mammalian developmental cell fusion systems. A deeper understanding of the precise regulation of fusion checkpoints, at the level of both signaling and membrane dynamics, could help develop new therapeutic strategies for genetic and acquired muscle diseases.

STAR Methods

Contact for Reagent and Resource Sharing

Further information and requests for resources and reagents should be directed to and will be fulfilled by the Lead Contact, Douglas Millay (douglas.millay@cchmc.org).

Experimental Model and Subject Details

Cells—C2C12 cells and 10T½ fibroblasts were purchased from American Type Culture Collection. Both cell types were propagated in DMEM (Gibco) containing 10% heat-inactivated bovine growth serum (BGS) and supplemented with penicillin-streptomycin (1%) at 37°C and 5% CO_2. Myomaker$^{-/-}$ and Myomerger$^{-/-}$ C2C12 cell lines were generated previously by using CRISPR/Cas9 mutageneisis (Millay et al., 2016; Quinn et al., 2017). Primary myoblasts were also generated previously (Millay et al., 2016; Quinn et al., 2017), and grown on collagen coated substrates but plated on fibronectin for differentiation. All myoblasts were differentiated by switching to DMEM containing 2% heat-inactivated horse serum (HS) and antibiotics. NIH 3T3 mouse fibroblasts of clone 15 cell line that stably express HA of Japan strain of influenza were a kind gift of Dr. Joshua Zimmerberg, NICHD, NIH (Wilson et al., 2015). These HA-expressing cells were cultured in DMEM with 10% FBS, 10^4 units/mL penicillin G, and 10 mg/mL streptomycin at 37°C and 5% CO_2. Human red blood cells (RBCs) were isolated from the blood of healthy donors (who had consented to participate in the NIH IRB-approved Research Donor Program in Bethesda, MD; all samples were anonymized).

Methods Details

Lipid and content mixing assays and synchronized fusion assays—We uncoupled the myoblast fusion stage of myogenic differentiation from the stages that prepare the cells for fusion using a fusion-synchronization approach described previously (Gamage et al., 2017; Leikina et al., 2013). In brief, fusion-committed myoblasts were placed into complete medium supplemented with 150 μM lauroyl LPC (#855475P, Avanti Polar Lipids). 16h later we washed the cells three times with LPC-free complete medium. C2C12 cells and primary myoblasts grown to 75% confluence in a 100 mm dish were labeled with either fluorescent lipid the Vybrant DiI or membrane-permeant Green CMFDA cell tracker or orange CMRA Cell Tracker (#V22885; #C7025 and #C34551, respectively, ThermoFisher Scientific), as recommended by the manufacturer and described previously (Leikina et al., 2013). These probes were also used to distinguish hemifusion and pore formation (described below) even when LPC was not used to synchronize cells.

We labeled C2C12 cells 48 hours after placement in the differentiation medium, and coplated differently labeled cells in a 1-to-1 ratio. For synchronized fusion, LPC was applied 2–3 hours after co-plating cells. The cells were incubated in the LPC-containing complete medium for 16 hours. Fusion was scored 30 min after LPC removal and thus ~68 hours after placing the cells into differentiation medium. In the experiments on murine primary myoblasts, we labeled proliferating cells in the growth medium. We co-plated differently labeled cells at 1-to-1 ratio and grew the cells in the growth medium for 16 more hours. Then we placed the cells into differentiation medium and 7 hours later applied LPC. We kept the cells in LPC-supplemented differentiation medium for 16 hours, washed out LPC with LPC-free medium and 30 minutes later (~24 hours after placing the cells into differentiation medium) scored fusion. Antibodies to Myomerger (sheep ESGP Ab # PA5-47639, ThermoFisher Sci.) or, in control experiments, sheep IgG-isotope control (#Ab37385, Abcam) were added to the LPC-free medium in which the cells were kept after LPC withdrawal.

Myoblast fusion assays and quantification—To specifically characterize different steps in fusion, we used 3 distinct assays: (i) hemifusion between cells labeled with membrane probe and content probe with unlabeled cells where hemifusion was detected as the appearance of lipid-labeled mononucleated cells without the content probe (Figure 1A, Figure 2A, Figure S1B)); (ii) opening of a fusion pore in fusion between cells labeled with green cell tracker and cells labeled with orange cell tracker was detected as appearance of double-labeled cells (Figure 1D); and (iii) fusion completion was detected as formation of multinucleated cells. As a control, we found no mononucleated cells labled with only membrane probe when cells labeled with both lipid and content probe as in (i) were incubated in the absence of unlabeled cells, showing that labled cells do not lose their content probe (data not shown). This indicates that when double labelled cells are mixed with unlabeled cells, the mononucleated cells labeled only with the lipid probe are indeed formed by hemifusion. Formation of multinucleated myotubes was quantified as the percentage of cell nuclei present in myotubes normalized to the total number of cell nuclei. Hemifusion and fusion pore opening were quantified as a number of double-labeled mononucleated cells normalized to the total number of cell nuclei in the field. For each condition, > 8 randomly chosen fields of view were imaged. We also analyzed fusion by assessing the number of nuclei in myosin+ cells. Here, cells were fixed with 4% paraformaldehyde (PFA)/PBS, permeabilized with 0.02% Triton X-100/PBS, and blocked with 3% BSA/PBS followed by immunostaining with myosin antibodies (MF 20, Developmental Studies Hybridoma Bank, 1:40) for one hour at room temperature. Alexa-Fluor secondary antibody (Invitrogen, 1:250) was incubated for 30 minutes at room temperature. Nuclei were stained with Hoechst (Invitrogen). Samples were imaged with a Nikon Eclipse inverted microscope with A1R confocal running NIS Elements and images were analyzed with Fiji (Schindelin et al., 2012).

Generation of recombinant Myomerger proteins—We generated recombinant proteins using either pMALX (Moon et al., 2010) or a modified pET28a backbone (generous gifts from Dr. Thomas Thompson, University of Cincinnati and Dr. Lars Pedersen, NIEHS, NIH). Each of these plasmids contains maltose binding protein (MBP) as an N-terminal

fusion protein, however the modified pET28a contains an N-terminal 6x histidine tag, thrombin cleavage site, and a PreScission Protease (PP) cleavage site after MBP. We cloned full-length Myomerger into pET28a-His-thrombin-MBP-PP and the ectodomain of Myomerger (amino acids 26-84) into both plasmids. The cDNA encoding full-length Myomerger or its ectodomain was obtained by amplifying the region from full-length Myomerger as a template. The above plasmids were transformed into *E. coli* BL21 (DE3) (Kattamuri et al., 2012) and grown in LB medium at 30°C supplemented with 50 μg ml^{-1} ampicillin for pMALX or 50 μg ml^{-1} kanamycin for pET28a-His-thrombin-MBP-PP, and once OD_{600} reached 0.6, protein expression was induced for 4 hours with 0.25 mM IPTG. Cells were lysed in protein purification buffer (20 mM Tris-HCl (pH 7.5), 300 mM NaCl, 1 mM EDTA) with sonication. The proteins were affinity purified with amylose resin (BioRad) and eluted with 20 mM maltose (Sigma-Aldrich) in protein purification buffer. The proteins without the PP site (in pMALX: MBP & MBPMyomerger$^{26\text{-}84}$) were further purified using a Superdex G200 Gel-Filtration column (GE Healthcare Life Sciences) in liposomal buffer (20 mM HEPES, pH 7.4 and 90 mM NaCl). Purity of the proteins was analyzed through SDS-PAGE followed by Coomassie Brilliant Blue G-250 staining (BioRad). Protein fractions containing proteins of interest were combined and concentrated with a 10K Molecular Weight Cutoff (MWCO) membrane (Pall Corporation). After eluting from the amylose resin, the proteins with the PP site (in pET28a-His-thrombin-MBP-PP: His-MBP-Myomerger$^{26\text{-}84}$) were incubated with PreScission protease (Sigma-Aldrich) overnight at 4°C. The cleaved protein was then dialyzed at 4°C overnight against cation exchange buffer (50 mM Sodium acetate pH 6.2) and was loaded onto a Mono S 5/5 cation exchange column (GE Healthcare Life Sciences). The protein was eluted with a linear NaCl gradient up to 1M to remove MBP and PP. Purity of the protein was analyzed through SDS-PAGE and the fractions containing Myomerger$^{26\text{-}84}$ were dialyzed with liposomal buffer and concentrated with a 3K Molecular Weight Cutoff (MWCO) membrane (Pall Corporation). Protein concentrations were measured using the Bradford method (BioRad) with BSA as a standard and aliquots were frozen in liquid nitrogen until further use.

Application of hypotonic osmotic shock, chlorpromazine, detergents, and recombinant protein—To assess an ability for osmotic stress to improve fusion, we treated the cells with PBS diluted by H_2O (1:3) as described (Chernomordik et al., 1998). To explore permeabilization of the plasma membrane of myoblasts we applied a strong hypotonic osmotic shock. We washed the cells with PBS and placed them in distilled water for 30 seconds at room temperature in the presence of Alexa Fluoro 488 phalloidin (#A12379, Invitrogen, final concentration of ~20 nM). Then we washed the cells in PBS and placed them into the complete medium for 10 minutes at 37°C in the presence of Hoechst 33342 (#H3570, ThermoFisher Sci., dilution 1:1000). After washing with PBS, we scored the percentage of permeabilized (phalloidin-labeled) cells using fluorescence microscopy.

Chlorpromazine CPZ (Sigma) was prepared as a 0.5 mM solution in PBS. At the time of LPC removal, synchronized WT, Myomaker$^{-/-}$ or Myomerger$^{-/-}$ C2C12 cells were placed into PBS supplemented with 50 μM CPZ for 60 seconds. Then the medium was replaced with differentiation medium for 30 minutes at 37°C. Fusi on (syncytium formation) extents

were compared with those in the control experiments, where the cells were treated with neither LPC nor CPZ.

For detergent and recombinant protein application, 2.5×10^4 myoblasts per well of an 8-well μ-slide (Ibidi) were differentiated for 72 hours. 0.06% Octyl-α-Glucoside (OG) (Anatrace) in differentiation media was incubated for 30 minutes at 37°2. Cells were washed with PBS and switched back to normal differentiation media for 5 hours. For primary myoblasts, 3×10^4 cells were plated per well of an 8-well μ-slide (Ibidi) coated with fibronectin (Sigma-Aldrich, 5 $\mu g/cm^2$) and differentiated for 36 hours. Cells were treated with 0.06% OG in PBS for 30 minutes at 37°2, washed with PBS and switched back to normal differentiation media for 2 hours. For recombinant proteins, cells were treated with various concentrations of rMBP or rMBP-Myomerger$^{26\text{-}84}$ (0.5 μM, 1.25 μM, 3 μM, 6.25 μM and 12.5 μM), or 6.25 μM of Magainin 2 (AnaSpec), in differentiation media for 20 hours at 37°C.

Membrane extraction—C2C12 cells were harvested on day 2 of differentiation in ice cold hypotonic buffer (TE buffer: 10 mM Tris-HCl pH 8, 2 mM EDTA) supplemented with complete protease inhibitor (Roche) and lysed using a dounce homogenizer. Lysates were then centrifuged at 800 × g for 5 minutes at 4°C to separate nuclei and cell debris. The supernatant was then centrifuged at 100,000 × g for one hour to isolate total membranes. The membrane pellets were resuspended in TE buffer, 1 M NaCl, 1 % SDS/TE, or in 0.1 M sodium carbonate (pH 11.5), and incubated on ice for 30 minutes with occasional vortexing. The membrane fractions were isolated at 100,000 × g for 1 hour and resuspended with RIPA buffer (50 mM Tris-HCl pH 7.4, 1% Triton X-100, 1% sodium deoxycholate, 1 mM EDTA, 0.1% SDS) at volumes equal to the supernatant. 10 μl of each fraction was separated by SDS-PAGE and analyzed for presence of Myomerger, Caveolin-3 (integral membrane protein), and Golgin 97 (peripheral membrane protein). The gel was transferred to a pre-equilibrated PVDF membrane (BioRad). The membrane was blocked with 5% milk in TBS-T (10 mM Tris-HCl pH 8.0, 150 mM NaCl)/0.05% Tween-20) for one hour at room temperature. After three washes with TBS-T, the membrane was incubated with primary antibodies/1% BSA overnight at 4°C. Myomerger antibody (R&D Systems #AF4580) was used at 1:200, Caveolin-3 antibody (BD Transduction Laboratories #610421) at 1:6700 and Golgin 97 (Cell Signaling Technologies #13192) at 1:1000. Membrane was then washed with TBS-T and incubated with Alexa Fluor 680 donkey anti-sheep secondary antibody (Invitrogen), Alexa Fluor 680 goat anti-mouse secondary antibody (Invitrogen) and IRDye 800CW goat anti-rabbit (LI-COR), respectively at 1:5000. Bands were visualized using the Odyssey® infrared detection system (LI-COR Biosciences).

Surface biotinylation—C2C12 cells (2 × 100 mm plates) were differentiated for two days and washed three times with cold PBS (137 mM NaCl, 2.7 mM KCl, 10 mM Na_2HPO_4, KH_2PO_4 pH 8.0). Cells were treated with 0.5 mg/mL EZ-link Sulfo-NHS-SS-Biotin (Pierce) at room temperature for 30 minutes. A control plate not exposed to EZ-link Sulfo-NHS-SS-Biotin was also processed. The cells were washed with PBS and non-reacted biotin was blocked with 50 mM Tris-HCl, pH 7.5. The cells were harvested with 1 mL of lysis buffer (10 mM Tris-HCl pH 7.5, 150 mM NaCl, 0.1% Triton X-100, 100 mM oxidized glutathione (Sigma-Aldrich), Protease Cocktail (Roche)) and were lysed with sonication five

times on ice. Samples were centrifuged at a speed of 15,000 rpm for 20 minutes and supernatants were incubated with magnetic streptavidin beads (Pierce) at room temperature for one hour to isolate biotinylated proteins. Beads were washed at least six times with the lysis buffer. For immunoblot analysis, 20 μL of RIPA buffer (50 mM Tris-HCl pH 7.4, 1% Triton X-100, 1% sodium deoxycholate, 1 mM EDTA, 0.1% SDS) was added along with 5 μL of 5× Laemmli loading buffer (300 mM Tris-HCl pH 6.8, 10% SDS, 50% glycerol, 0.25% bromophenol blue) to the beads and heated at 95Ό for 5 minutes. Western blotting was performed as described above for Myomerger and Tubulin. Tubulin (Santa Cruz #sc-8035) was used at 1:50.

Liposome preparation and assays—The lipids used in this study were dioleoylphosphatidylcholine (DOPC) and dioleoylphosphatidylserine (DOPS), 1,2-distearoly-sn-glycero-3-phosphoethanolamine-N-[amino(polyethylene glycol)-2000] (ammonium salt) (DSPE-PEG (2000)) from Avanti Polar Lipids. DiI and DiD (Invitrogen) were used as lipid dyes for lipid mixing experiments. For leakage experiments in Figures 5B, 5C, the liposomes were processed as previously described (Kyoung et al., 2013). Briefly, the lipids were mixed to a final concentration of 10 mM with a molar ratio of 70:30 (DOPC:DOPS) and were dried under vacuum to form a lipid film on the wall of a glass tube. The dried lipid film was resuspended in liposomal buffer (20 mM HEPES, 90 mM NaCl, pH 7.4) with 50 mM sulforhodamine B (Sigma-Aldrich). After three freeze–thaw cycles, the labeled liposomes were isolated using a NAP-25 column (GE healthcare) which also removed free sulforhodamine B. For leakage experiments decribed in Figures S5C, S5E the liposomes were prepared through freeze-thaw followed by extrusion. In brief, the mixtures DOPC:DOPS (molar ratio 70:30) or DOPC:DOPS:PEG-PE (molar ratio 68:30:2) were dried under vacuum in a glass tube and the dried lipid film was hydrated in liposomal buffer with 50 mM sulforhodamine B. For the lipid mixing experiments described in Figure S5F, lipids were mixed to obtain DOPC:DOPS ((unlabeled) molar ratio 70:30), DOPC:DOPS:DiI:DiD ((labeled) molar ratio 66:30:2:2), DOPC:DOPS:PEG-PE ((unlabeled) molar ratio 68:30:2) DOPC:DOPS:PEG-PE:DiI:DiD ((labeled) molar ratio 64:30:2:2:2) and the dried lipid film was suspeneded in liposomal buffer. The resulting lipid suspensions were submitted to five freeze-thaw cycles followed by 25 extrusions through polycarbonate filters (100 nm pore size, Avanti Polar Lipids) using a mini-extruder (Avanti Polar Lipids) to produce large unilamellar vesicles (LUVs). Details of the leakage assay have previously been described (Crowe et al., 2017). Experiments were performed using a Gemini XPS plane reader (Molecular Devices) with a 96-well microplate (Corning Inc). Fluorescence from the sulforhodamine B labeled liposomes was measured every 7 seconds for 15 minutes after the addition of proteins. All measurements were performed at room temperature. The excitation and emission wavelengths were 544 and 590 nm, respectively. The emission fluorescence for each time point was measured as F_n. The emission fluorescence of the untreated liposomes was measured as F_0, and that of the liposomes solubilized with 0.1% SDS was defined as F_{100}. The percentage of liposome leakage at each time point is defined as: liposome leakage (% of SDS) = $(F_n - F_0) \times 100/(F_{100} - F_0)$. For lipid mixing eperiments, labeled and unlabeled liposomes were mixed at a ratio of 1:9 to obtain a final lipid concentration of 100 μM (outer leaflet concentration was 50 μM). Fluorescence intensities were monitored every 20 seconds for 15 minutes after adding the protein in two channels with the excitation

wavelength of 530 nm and emission wavelengths of 570 and 670 nm for donor DiI and acceptor DiD respectively. Fluorescence changes for donor (DiI) emission were plotted as a percentage of SDS quenching. All measurements were performed at room temperature.

Dox-inducible cell fusion reconstitution—Viruses were generated using a procedure adapted from the Broad Institute protocol; briefly, 293T cells (passages ≤15) were seeded in culture medium (DMEM, 10% FCS, 1% Pen-Strep) at 3.8×10^6 cells/100 mm plates. After 18 hours, culture medium was replaced with 9.5 mL of antibiotic-free medium (DMEM, 10% FCS, without Pen-Strep). The transfection reaction mixture was prepared by mixing and incubating plasmid DNA (7.5 μg transfer, 4.8 μg packaging, 2.7 μg envelope) with Fugene6 (Promega: 3 μL:1 μg DNA) in 500 μL of serum-free antibiotic-free DMEM for 20 minutes at room temperature. This reaction mixture was then dispersed over the 293T cells 24 hours after seeding and transfection carried out for 16-18 hours at 37°C. The transfection medium was replaced with virus-harvesting medium (DMEM, 20% FCS, 1% Pen-Strep) and virus generation allowed to proceed for 48 hours. Supernatants were harvested, filtered through 0.45 μm syringe filters, and overlaid on cells for transduction. Identical protocols were followed for generation of both Myomaker-encoding retroviruses (using pBX-myomaker transfer vector (Millay et al., 2013) and Gag/Pol packaging constructs (Addgene)) and Myomerger-encoding lentiviruses (using the psPAX2 packaging construct (Addgene)). For both we also included the envelope plasmid, pCMV-VSV-G (Addgene). cDNA for Myomerger (Quinn et al., 2017) and Myomerger-FLAG was cloned into the pLVX-TetONE-Puro transfer vector (Clonetech) to achieve Doxycycline (dox)-inducible expression of Myomerger in transduced cells that would also be constitutively puromycin-resistant. To generate Myomerger$^{\Delta 1\text{-}25}$, amino acids 1-25 were replaced with a synthetic cleavable signal sequence from influenza virus hemaglutinnin using standard PCR-based mutagenesis and this construct was cloned into the pBabe-X plasmid. All recombinant plasmids were confirmed by sequenceing prior to use and primers can be found on the Key Resources page.

Transduction of 10T½ fibroblasts was achieved by seeding at 10^5 cells/well in a 6-well format in 2 mL of complete medium (DMEM, 10% BGS, 1% Pen-Strep) and incubated overnight at 37°C. On the next day, cells were serially transduced with retro-Myomaker and lenti-Myomerger viruses using a spinfection protocol; briefly, cells were initially overlaid with 2.5 mL of undiluted retrovirus-containing medium supplemented with 6 μg/mL polybrene and subjected to centrifugation (652 × g in a swinging bucket rotor) at 23°C for 60 minutes. Infection was continued at 37°C for an additional 12 hours, after which the spinfection protocol was repeated with the inducible Myomerger-encoding lentivirus. After a cumulative ~24-hour transduction period, cells were returned to complete medium. Exposure to selection medium (complete medium, 4 μg/mL puromycin) was started 48 hours after lentiviral transduction was initiated and proceeded for 2 days. Surviving cells were trypsinized (0.05% trypsin), propagated in complete medium on a 3-day/passage cycle, and subjected to the 2 day puromycin-selection protocol every 2-3 passages. Fusogenic capability, protein expression, and co-immunoprecipitations were assessed in passages 3-5 or later. Assessment of protein expression was achieved by seeding cells in a 12-well format (5×10^4 cells/well) in complete medium on day 0, and treated with ±dox containing medium

beginning on day 1 for 48 hours. Cells were then rapidly washed twice in ice-cold 1× PBS, directly lysed in 50 μL of 1× Laemmli buffer containing 100mM DTT; lysates were heated at 95°C for 10 minutes before being subjected to immunoblot analyses as described above.

To assess fusion reconstitution, transduced 10T½ fibroblasts were seeded in 8-chamber Ibidi slides at 5×10^3 cells/chamber (300 μL complete medium) on day 0 and incubated overnight. On day 1 (~16-18 hours post-seeding), Myomerger expression was induced by treating cells in experimental chambers with dox containing complete medium (1 μg/mL), while control chambers received normal (−dox) medium. Media (±dox) was replaced once at 36-hour time point and assay allowed to proceed for a total of 72 hours of dox treatment at which time fusion was evaluated.

Co-Immunoprecipitations and super-resolution microscopy—Retrovirus used for acute infection (Figure S6A) was generated from Platinum E cells (Cell Biolabs), which were transfected with combinations of pBX-Empty, pBX-Myomerger (Quinn et al., 2017), or pBX-FLAG-Myomaker (Millay et al., 2016) (10 μg total DNA), and virus was collected 48 hours after transfection. Viral supernatants were filtered through a 0.45 μm syringe filter and incubated with fibroblasts or myoblasts (C2C12) for 18 hours. Viral media was replaced with normal growth media and cells were harvested 72 hours after infection. FLAG-Myomaker contains a cleavable, synthetic signal sequence followed by the FLAG epitope then full-length Myomaker (Millay et al., 2016). For all immunoprecipitations, cells were washed with ice cold PBS, scraped into a conical tube, pelleted and resuspended in 1 ml of Buffer 1 (50 mM Tris-HCl pH 7.4, 150 mM NaCl, 1 mM EDTA, 0.1% Triton X-100) supplemented with complete protease inhibitor (Roche). Cells were incubated for 15 minutes, passed through a 27G 1/2 needle 10 times, and mixed for 1 hour at 4Ό. To immunoprecipitate FLAG tagged proteins, the supernatants were collected by centrifugation at 21,000 × g for 15 minutes and incubated with 50 μL of pre-washed Anti-FLAG M2 affinity resin (Sigma) for ~16 hours at 4°C. To immunoprecipitate untagged Myomerger, the supernatants were collected by centrifugation at 1000 × g for 15 min and pre-cleared by incubation with Protein A Dynabeads (Life Technologies) for 2 hours at 4°C. To generate the antibody-bead mix, 6 μg of Myomerger antibodies were incubated with 50 μL of pre-washed Protein A Dynabeads for 2 hours at 4°C. The antibody-beads were washed thrice in Buffer 1 and incubated with the pre-cleared supernatant for ~ 16 hours at 4°C. The beads were then washed with high salt (50 mM Tris, 700 mM NaCl, 1 mM EDTA) buffer, followed by three washes with Buffer 1. Immunoprecipitated proteins were eluted using 30 μL of RIPA buffer (50 mM Tris-HCl pH 7.4, 1% Triton X-100, 1% sodium deoxycholate, 1 mM EDTA, 0.1% SDS) along with 6 μL of 5× Laemmli loading buffer. The beads were heated at 95°C for 5 minutes and separated by SDS-PAGE and analyzed for presence of Myomaker, Myomerger, and GAPDH (as a loading control (Milipore; 1:10,000)) . 10% of the total cells were lysed in SDS buffer (50 mM Tris-HCl pH 6.8, 1 mM EDTA, 2% SDS) and used as inputs.

Super-resolution microscopy was performed with a Nikon A1 LUN-A inverted confocal microscopy. C2C12 myoblasts were differentiated for two days and immunostained with custom Myomaker antibodies (Gamage et al., 2017) and Myomerger antibodes described above. Images were acquired with a 100X objective NA1.45 at 4 times the Nyquist limit

(0.03 μm pixel size). Z- stacks were acquired using a 0.4 AU pinhole yielding a 0.35 μm optical section at 0.1 μm intervals and 2X integration to avoid pixel saturation. Images were deconvolved with NIS elements using 15 iterations of the Landweber method. Images shown are a single focal plane.

HA-mediated cell fusion experiments—To examine effects of Myomaker and Myomerger expression on fusion mediated by influenza hemagglutinin (HA) we used NIH 3T3 mouse fibroblasts of clone 15 cell line that stably express HA of Japan strain of influenza (Wilson et al., 2015). HA^+ cells were cultured in DMEM supplemented with 10% heat-inactivated FBS and antibiotics at 37°C and 5% CO_2. The cells (HA^+ cells) express an uncleaved precursor form of HA, HA0, which is fusion-incompetent but mediates binding of HA^+ cells to red blood cells (RBCs) via HA0 interactions with sialic acid receptors at the surface of RBCs. We labeled RBCs with the fluorescent lipid PKH26 (Sigma) and loaded with carboxyfluorescein, CF (5-(and-6)-Carboxyfluorescein, mixed isomers, #C368, Invitrogen), as described in (Chernomordik et al., 1998) and prepared HA^+ for the experiments by treating them with trypsin to cleave HA0 into the fusion-competent HA1-S-S-HA2 form. In contrast to the optimized trypsin pre-treatment (5 μg/ml, 10 minutes, room temperature) that cleaves most of the cell-surface HAs (Chernomordik et al., 1998), we applied a lower concentration of trypsin for a shorter time (1 μg/ml trypsin, 2 minutes, room temperature) to cleave only a fraction of all HA0 molecules at the surface of HA-cells. After two washings with PBS, cells were incubated for 10 min with a 1 ml suspension of RBCs (0.05% hematocrit). HA-expressing cells with zero to two bound RBC per cell were washed three times with PBS to remove unbound RBC and then used. HA-cells with 0–2 bound RBCs per cell were treated with the low pH medium (PBS titrated with citrate to the pH 5.15 for 5 min at 37Ό). Low pH application was ended by replacement of the acidic solution with PBS. We assayed complete fusion and hemifusion in HA^+ fibroblast/RBC fusion by fluorescence microscopy as (i) the ratio of content probe-redistributed bound RBCs to the total number of bound RBCs and (ii) the ratio of lipid-redistributed but not content-mixing bound RBCs to the total number of bound RBCs, respectively. For each condition, we imaged and analyzed ≥ 30 randomly chosen fields of view (15-30 RBC-fibroblast pairs per field).

24 hours before fusion experiments, HA-cells at ~50% confluency were transfected with 2 μg/ml of pcDNA3-Myomaker, pcDNA3-Myomerger, or pcDNA3-empty per 35×10 mm^2 plate using Lipofectamine 3000. In parallel experiments, we transfected the cells with GFP vector and, based on GFP expression, estimated the transfection efficiency to be >60%. Using immunofluorescence microscopy, we verified expression of Myomaker or Myomerger in HA^+ cells by fixing the cells with 4% formaldehyde (10 minutes, room temperature). The cells were then washed with PBS and then treated with 0.1% Triton X-100 in PBS for 3 minutes at room temperature. After 3 washes with PBS, we blocked non-specific binding by treating the cells with 10% FBS in PBS for 10 minutes and then applied primary antibodies to either Myomaker (Abcam, Anti-TMEM8C antibody (#ab188300) at 1:50 dilution) or Myomerger antibodies (sheep Anti-ESGP antibody, ESGP Ab # PA5-47639, ThermoFisher Sci. at 1:100 dilution). The cells were incubated with primary antibodies for 1 hour at room temperature, washed 4 times, blocked with 10% FBS in PBS for 10 minutes and then

incubated with secondary Alexa 647 goat anti-rabbit or donkey anti-sheep for Myomaker and Myomerger antibodies, respectively. In control experiments, neither lipid- nor content mixing was observed for either HA^+ $Myomerger^+$ fibroblasts or HA^+ $Myomaker^+$ fibroblasts that were not treated with trypsin or not treated with low pH (data not shown). Thus, on their own, neither Myomerger nor Myomaker initiates fusion of pre-docked membranes.

Quantification and Statistical Analysis

To quantify each experiment, at least 3 independent experiments were performed in duplicate and ≥ 5 randomly chosen fields of view were imaged (unless stated otherwise in the figure legend). At least 150 cells were counted manually for each image. We initially assessed the distribution of the data with a Shapiro-Wilk normality test. If the data were normally distributed, we used a parametric two-tailed t-test to determine significance. Data that were non-normally distributed were analyzed with a non-parametric Mann-Whitney test to determine significance. Data are presented in box-and-whisker plots where the center lines show the median, box the 25^{th}-75^{th} percentiles, and whiskers the maximum and minimum values, or in dot plots with mean and standard deviation. These statistical analyses were performed using the GraphPad Prism 6 software. The criterion for statistical significance was $P < 0.05$ ($*P < 0.05$, $**P < 0.01$, $***P < 0.001$, $****P < 0.0001$).

Supplementary Material

Refer to Web version on PubMed Central for supplementary material.

Acknowledgements

We thank Malgorzata Quinn from the Millay laboratory, Yanchong Hu from the Diao laboratory, and the Thompson laboratory (University of Cincinnati) for technical assistance, and Kamran Melikov from the Chernomordik laboratory for helpful discussions. This work was supported by grants to D.P.M. from the Cincinnati Children's Hospital Research Foundation, National Institutes of Health (R01AR068286), and Pew Charitable Trusts. The research in L.V.C. laboratory was supported by the Intramural Research Program of the Eunice Kennedy Shriver National Institute of Child Health and Human Development, National Institutes of Health and by Grant Number 2013151 from the United States - Israel Binational Science Foundation (BSF).

References

Beck T, Delley PA, and Hall MN (2001). Control of the actin cytoskeleton by extracellular signals. Results Probl Cell Differ 32, 231–262. [PubMed: 11131835]

Bi P, McAnally JR, Shelton JM, Sanchez-Ortiz E, Bassel-Duby R, and Olson EN (2018). Fusogenic micropeptide Myomixer is essential for satellite cell fusion and muscle regeneration. Proc Natl Acad Sci U S A 115, 3864–3869. [PubMed: 29581287]

Bi P, Ramirez-Martinez A, Li H, Cannavino J, McAnally JR, Shelton JM, Sanchez-Ortiz E, Bassel-Duby R, and Olson EN (2017). Control of muscle formation by the fusogenic micropeptide myomixer. Science 356, 323–327. [PubMed: 28386024]

Blijleven JS, Boonstra S, Onck PR, van der Giessen E, and van Oijen AM (2016). Mechanisms of influenza viral membrane fusion. Semin Cell Dev Biol 60, 78–88. [PubMed: 27401120]

Chernomordik LV, Frolov VA, Leikina E, Bronk P, and Zimmerberg J (1998). The pathway of membrane fusion catalyzed by influenza hemagglutinin: restriction of lipids, hemifusion, and lipidic fusion pore formation. J Cell Biol 140, 1369–1382. [PubMed: 9508770]

Chernomordik LV, and Kozlov MM (2003). Protein-lipid interplay in fusion and fission of biological membranes. Annu Rev Biochem 72, 175–207. [PubMed: 14527322]

Ciechonska M, and Duncan R (2014). Reovirus FAST proteins: virus-encoded cellular fusogens. Trends Microbiol 22, 715–724. [PubMed: 25245455]

Cohen FS, and Melikyan GB (2004). The energetics of membrane fusion from binding, through hemifusion, pore formation, and pore enlargement. J Membr Biol 199, 1–14. [PubMed: 15366419]

Crowe M, Lai Y, Wang Y, Lu J, Zhao M, Tian Z, Long J, Zhang P, and Diao J (2017). A Proteoliposome Method for Assessing Nanotoxicity on Synaptic Fusion and Membrane Integrity. Small Methods 1.

Cummings JE, and Vanderlick TK (2007). Aggregation and hemi-fusion of anionic vesicles induced by the antimicrobial peptide cryptdin-4. Biochim Biophys Acta 1768, 1796–1804. [PubMed: 17531950]

Demonbreun AR, Biersmith BH, and McNally EM (2015). Membrane fusion in muscle development and repair. Semin Cell Dev Biol 45, 48–56. [PubMed: 26537430]

Deng S, Azevedo M, and Baylies M (2017). Acting on identity: Myoblast fusion and the formation of the syncytial muscle fiber. Semin Cell Dev Biol 72, 45–55. [PubMed: 29101004]

Di Gioia SA, Connors S, Matsunami N, Cannavino J, Rose MF, Gilette NM, Artoni P, de Macena Sobreira NL, Chan WM, Webb BD, et al. (2017). A defect in myoblast fusion underlies Carey-Fineman-Ziter syndrome. Nat Commun 8, 16077. [PubMed: 28681861]

Duan R, and Gallagher PJ (2009). Dependence of myoblast fusion on a cortical actin wall and nonmuscle myosin IIA. Dev Biol 325, 374–385. [PubMed: 19027000]

Duan R, Jin P, Luo F, Zhang G, Anderson N, and Chen EH (2012). Group I PAKs function downstream of Rac to promote podosome invasion during myoblast fusion in vivo. J Cell Biol 199, 169–185. [PubMed: 23007650]

Fedry J, Liu Y, Pehau-Arnaudet G, Pei J, Li W, Tortorici MA, Traincard F, Meola A, Bricogne G, Grishin NV, et al. (2017). The Ancient Gamete Fusogen HAP2 Is a Eukaryotic Class II Fusion Protein. Cell 168, 904–915 e910. [PubMed: 28235200]

Finkelstein A, Zimmerberg J, and Cohen FS (1986). Osmotic swelling of vesicles: its role in the fusion of vesicles with planar phospholipid bilayer membranes and its possible role in exocytosis. Annu Rev Physiol 48, 163–174. [PubMed: 2423021]

Gamage DG, Leikina E, Quinn ME, Ratinov A, Chernomordik LV, and Millay DP (2017). Insights into the localization and function of myomaker during myoblast fusion. J Biol Chem 292, 17272–17289. [PubMed: 28860190]

Gruenbaum-Cohen Y, Harel I, Umansky KB, Tzahor E, Snapper SB, Shilo BZ, and Schejter ED (2012). The actin regulator N-WASp is required for muscle-cell fusion in mice. Proc Natl Acad Sci U S A 109, 11211–11216. [PubMed: 22736793]

Guan XM, Peroutka SJ, and Kobilka BK (1992). Identification of a single amino acid residue responsible for the binding of a class of beta-adrenergic receptor antagonists to 5-hydroxytryptamine1A receptors. Mol Pharmacol 41, 695–698. [PubMed: 1349154]

Hamoud N, Tran V, Croteau LP, Kania A, and Cote JF (2014). G-protein coupled receptor BAI3 promotes myoblast fusion in vertebrates. Proc Natl Acad Sci U S A 111, 3745–3750. [PubMed: 24567399]

Hernandez JM, and Podbilewicz B (2017). The hallmarks of cell-cell fusion. Development 144, 4481–4495. [PubMed: 29254991]

Hochreiter-Hufford AE, Lee CS, Kinchen JM, Sokolowski JD, Arandjelovic S, Call JA, Klibanov AL, Yan Z, Mandell JW, and Ravichandran KS (2013). Phosphatidylserine receptor BAI1 and apoptotic cells as new promoters of myoblast fusion. Nature 497, 263–267. [PubMed: 23615608]

Horsley V, Jansen KM, Mills ST, and Pavlath GK (2003). IL-4 acts as a myoblast recruitment factor during mammalian muscle growth. Cell 113, 483–494. [PubMed: 12757709]

Ivanovic T, and Harrison SC (2015). Distinct functional determinants of influenza hemagglutinin-mediated membrane fusion. Elife 4, e11009. [PubMed: 26613408]

Jahn R, and Sudhof TC (1999). Membrane fusion and exocytosis. Annu Rev Biochem 68, 863–911. [PubMed: 10872468]

Kattamuri C, Luedeke DM, Nolan K, Rankin SA, Greis KD, Zorn AM, and Thompson TB (2012). Members of the DAN family are BMP antagonists that form highly stable noncovalent dimers. J Mol Biol 424, 313–327. [PubMed: 23063586]

Kielian M, and Rey FA (2006). Virus membrane-fusion proteins: more than one way to make a hairpin. Nat Rev Microbiol 4, 67–76. [PubMed: 16357862]

Kyoung M, Zhang Y, Diao J, Chu S, and Brunger AT (2013). Studying calcium-triggered vesicle fusion in a single vesicle-vesicle content and lipid-mixing system. Nat Protoc 8, 1–16. [PubMed: 23222454]

Leikina E, and Chernomordik LV (2000). Reversible merger of membranes at the early stage of influenza hemagglutinin-mediated fusion. Mol Biol Cell 11, 2359–2371. [PubMed: 10888674]

Leikina E, Melikov K, Sanyal S, Verma SK, Eun B, Gebert C, Pfeifer K, Lizunov VA, Kozlov MM, and Chernomordik LV (2013). Extracellular annexins and dynamin are important for sequential steps in myoblast fusion. J Cell Biol 200, 109–123. [PubMed: 23277424]

Leikina E, Mittal A, Cho MS, Melikov K, Kozlov MM, and Chernomordik LV (2004). Influenza hemagglutinins outside of the contact zone are necessary for fusion pore expansion. J Biol Chem 279, 26526–26532. [PubMed: 15078874]

Matsuzaki K, Sugishita K, Ishibe N, Ueha M, Nakata S, Miyajima K, and Epand RM (1998). Relationship of membrane curvature to the formation of pores by magainin 2. Biochemistry 37, 11856–11863. [PubMed: 9718308]

Melikyan GB, Brener SA, Ok DC, and Cohen FS (1997). Inner but not outer membrane leaflets control the transition from glycosylphosphatidylinositol-anchored influenza hemagglutinin-induced hemifusion to full fusion. J Cell Biol 136, 995–1005. [PubMed: 9060465]

Melikyan GB, White JM, and Cohen FS (1995). GPI-anchored influenza hemagglutinin induces hemifusion to both red blood cell and planar bilayer membranes. J Cell Biol 131, 679691.

Millay DP, Gamage DG, Quinn ME, Min YL, Mitani Y, Bassel-Duby R, and Olson EN (2016). Structure-function analysis of myomaker domains required for myoblast fusion. Proc Natl Acad Sci U S A 113, 2116–2121. [PubMed: 26858401]

Millay DP, O'Rourke JR, Sutherland LB, Bezprozvannaya S, Shelton JM, Bassel-Duby R, and Olson EN (2013). Myomaker is a membrane activator of myoblast fusion and muscle formation. Nature 499, 301–305. [PubMed: 23868259]

Millay DP, Sutherland LB, Bassel-Duby R, and Olson EN (2014). Myomaker is essential for muscle regeneration. Genes Dev 28, 1641–1646. [PubMed: 25085416]

Moon AF, Mueller GA, Zhong X, and Pedersen LC (2010). A synergistic approach to protein crystallization: combination of a fixed-arm carrier with surface entropy reduction. Protein Sci 19, 901–913. [PubMed: 20196072]

Muller M, and Schick M (2011). An alternate path for fusion and its exploration by field-theoretic means. Curr Top Membr 68, 295–323. [PubMed: 21771504]

Nazari M, Kurdi M, and Heerklotz H (2012). Classifying surfactants with respect to their effect on lipid membrane order. Biophys J 102, 498–506. [PubMed: 22325272]

Nguyen AN, Song JA, Nguyen MT, Do BH, Kwon GG, Park SS, Yoo J, Jang J, Jin J, Osborn MJ, et al. (2017). Prokaryotic soluble expression and purification of bioactive human fibroblast growth factor 21 using maltose-binding protein. Sci Rep 7, 16139. [PubMed: 29170489]

Nowak SJ, Nahirney PC, Hadjantonakis AK, and Baylies MK (2009). Nap1-mediated actin remodeling is essential for mammalian myoblast fusion. J Cell Sci 122, 3282–3293. [PubMed: 19706686]

Patel H, Huynh Q, Barlehner D, and Heerklotz H (2014). Additive and synergistic membrane permeabilization by antimicrobial (lipo)peptides and detergents. Biophys J 106, 2115–2125. [PubMed: 24853740]

Perez-Vargas J, Krey T, Valansi C, Avinoam O, Haouz A, Jamin M, Raveh-Barak H, Podbilewicz B, and Rey FA (2014). Structural basis of eukaryotic cell-cell fusion. Cell 157, 407–419. [PubMed: 24725407]

Pietuch A, Bruckner BR, and Janshoff A (2013). Membrane tension homeostasis of epithelial cells through surface area regulation in response to osmotic stress. Biochim Biophys Acta 1833, 712–722. [PubMed: 23178740]

Podbilewicz B (2014). Virus and cell fusion mechanisms. Annu Rev Cell Dev Biol 30, 111–139. [PubMed: 25000995]

Podbilewicz B, Leikina E, Sapir A, Valansi C, Suissa M, Shemer G, and Chernomordik LV (2006). The C. elegans developmental fusogen EFF-1 mediates homotypic fusion in heterologous cells and in vivo. Dev Cell 11, 471–481. [PubMed: 17011487]

Quinn ME, Goh Q, Kurosaka M, Gamage DG, Petrany MJ, Prasad V, and Millay DP (2017). Myomerger induces fusion of non-fusogenic cells and is required for skeletal muscle development. Nat Commun 8, 15665. [PubMed: 28569755]

Rand RP, Kachar B, and Reese TS (1985). Dynamic morphology of calcium-induced interactions between phosphatidylserine vesicles. Biophys J 47, 483–489. [PubMed: 3986279]

Randrianarison-Huetz V, Papaefthymiou A, Herledan G, Noviello C, Faradova U, Collard L, Pincini A, Schol E, Decaux JF, Maire P, et al. (2017). Srf controls satellite cell fusion through the maintenance of actin architecture. J Cell Biol.

Sampath SC, Sampath SC, and Millay DP (2018). Myoblast fusion confusion: the resolution begins. Skelet Muscle 8, 3. [PubMed: 29386054]

Schejter ED (2016a). Myoblast fusion: Experimental systems and cellular mechanisms. Semin Cell Dev Biol.

Schejter ED (2016b). Myoblast fusion: Experimental systems and cellular mechanisms. Semin Cell Dev Biol 60, 112–120. [PubMed: 27423913]

Schindelin J, Arganda-Carreras I, Frise E, Kaynig V, Longair M, Pietzsch T, Preibisch S, Rueden C, Saalfeld S, Schmid B, et al. (2012). Fiji: an open-source platform for biological-image analysis. Nat Methods 9, 676–682. [PubMed: 22743772]

Schmid SL, and Frolov VA (2011). Dynamin: functional design of a membrane fission catalyst. Annu Rev Cell Dev Biol 27, 79–105. [PubMed: 21599493]

Schwander M, Leu M, Stumm M, Dorchies OM, Ruegg UT., Schittny J., and Muller U (2003). Beta1 integrins regulate myoblast fusion and sarcomere assembly. Dev Cell 4, 673–685. [PubMed: 12737803]

Sens KL, Zhang S, Jin P, Duan R, Zhang G, Luo F, Parachini L, and Chen EH (2010). An invasive podosome-like structure promotes fusion pore formation during myoblast fusion. J Cell Biol 191, 1013–1027. [PubMed: 21098115]

Shi J, Bi P, Pei J, Li H, Grishin NV, Bassel-Duby R, Chen EH, and Olson EN (2017). Requirement of the fusogenic micropeptide myomixer for muscle formation in zebrafish. Proc Natl Acad Sci U S A 114, 11950–11955. [PubMed: 29078404]

Shilagardi K, Li S, Luo F, Marikar F, Duan R, Jin P, Kim JH, Murnen K, and Chen EH (2013). Actin-propelled invasive membrane protrusions promote fusogenic protein engagement during cell-cell fusion. Science 340, 359–363. [PubMed: 23470732]

Valansi C, Moi D, Leikina E, Matveev E, Grana M, Chernomordik LV, Romero H, Aguilar PS, and Podbilewicz B (2017). Arabidopsis HAP2/GCS1 is a gamete fusion protein homologous to somatic and viral fusogens. J Cell Biol 216, 571–581. [PubMed: 28137780]

Vasyutina E, Martarelli B, Brakebusch C, Wende H, and Birchmeier C (2009). The small G-proteins Rac1 and Cdc42 are essential for myoblast fusion in the mouse. Proc Natl Acad Sci U S A 106, 8935–8940. [PubMed: 19443691]

Verma SK, Leikina E, Melikov K, and Chernomordik LV (2014). Late stages of the synchronized macrophage fusion in osteoclast formation depend on dynamin. Biochem J 464, 293–300. [PubMed: 25336256]

Weber T, Zemelman BV, McNew JA, Westermann B, Gmachl M, Parlati F, Sollner TH, and Rothman JE (1998). SNAREpins: minimal machinery for membrane fusion. Cell 92, 759–772. [PubMed: 9529252]

Wen X, Saltzgaber GW, and Thoreson WB (2017). Kiss-and-Run Is a Significant Contributor to Synaptic Exocytosis and Endocytosis in Photoreceptors. Front Cell Neurosci 11, 286. [PubMed: 28979188]

White JM, Delos SE, Brecher M, and Schornberg K (2008). Structures and mechanisms of viral membrane fusion proteins: multiple variations on a common theme. Crit Rev Biochem Mol Biol 43, 189–219. [PubMed: 18568847]

Wilson RL, Frisz JF, Klitzing HA, Zimmerberg J, Weber PK, and Kraft ML (2015). Hemagglutinin clusters in the plasma membrane are not enriched with cholesterol and sphingolipids. Biophys J 108, 1652–1659. [PubMed: 25863057]

Xu Y, Zhang F, Su Z, McNew JA, and Shin YK (2005). Hemifusion in SNARE-mediated membrane fusion. Nature structural & molecular biology 12, 417–422.

Yang ST, Zaitseva E, Chernomordik LV, and Melikov K (2010). Cell-penetrating peptide induces leaky fusion of liposomes containing late endosome-specific anionic lipid. Biophys J 99, 2525–2533. [PubMed: 20959093]

Zhang Q, Vashisht AA, O'Rourke J, Corbel SY, Moran R, Romero A, Miraglia L, Zhang J, Durrant E, Schmedt C, et al. (2017). The microprotein Minion controls cell fusion and muscle formation. Nat Commun 8, 15664. [PubMed: 28569745]

Highlights

3-4 bullet points of no more than 85 characters in length (including spaces) they summarize the core results of the paper in order to allow readers to quickly gain an understanding of the main take-home messages.

- Myomaker and Myomerger govern distinct phases of the fusion pathway in myoblasts
- Myomaker is essential for hemifusion of the plasma membranes
- Myomerger ectodomains drive fusion pore formation by generating membrane stresses
- Fusogenic activities of these proteins do not require a direct interaction

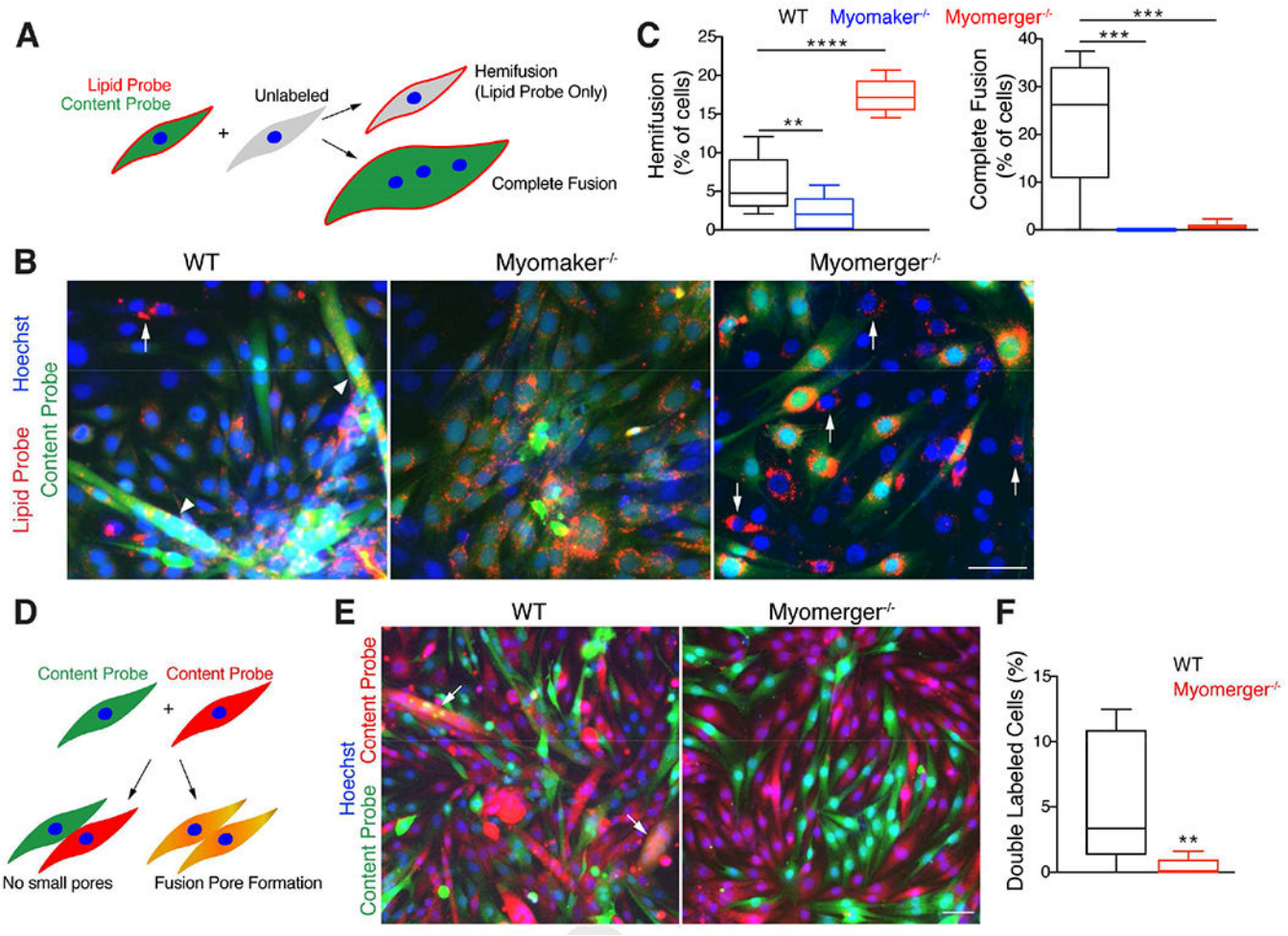

Figure 1. Distinct roles for Myomaker and Myomerger during the fusion process.

(A) Unsynchronized cell fusion assay (no LPC) to monitor lipid and content mixing. Cells are differentiated for 48 hours then one population is labeled with both lipid (red, DiI) and content (green cell tracker) probes and mixed with unlabeled cells. Hemifusion is identified as mononucleated cells with only the red lipid probe whereas complete fusion is identified as multinucleated cells with both probes, and these indices were scored 24 hours after mixing the labeled and unlabeled cells. (B) Immunofluorescence images of WT, Myomaker$^{-/-}$ and Myomerger$^{-/-}$ C2C12 myoblasts after lipid and content mixing. Arrows indicate hemifused cells, whereas arrowheads mark complete fusion. (C) Quantification of hemifusion (left, n=3 independent experiments) and complete fusion (right, n=3 independent experiments) as a percentage to total cells. (D) Schematic of content mixing to assess formation of fusion pores. (E) Fusion pore formation was identified by the appearance of double labeled cells (arrows) in WT and Myomerger$^{-/-}$ C2C12 myoblasts after 24 hours. (F) Quantification of (E) (n=3 independent experiments) as a percentage of total cells. Statistical analyses and data presentation: (C) (Hemifusion), two tailed Student's t-test; (C) (complete fusion), (F), Mann-Whitney test; box-and-whisker plots show median (center line), 25th–75th percentiles (box) and minimum and maximum values (whiskers); $^{**}P < 0.01$, $^{***}P < 0.001$, $^{****}P < 0.0001$. Scale bars, 50 μm. See also Figure S1.

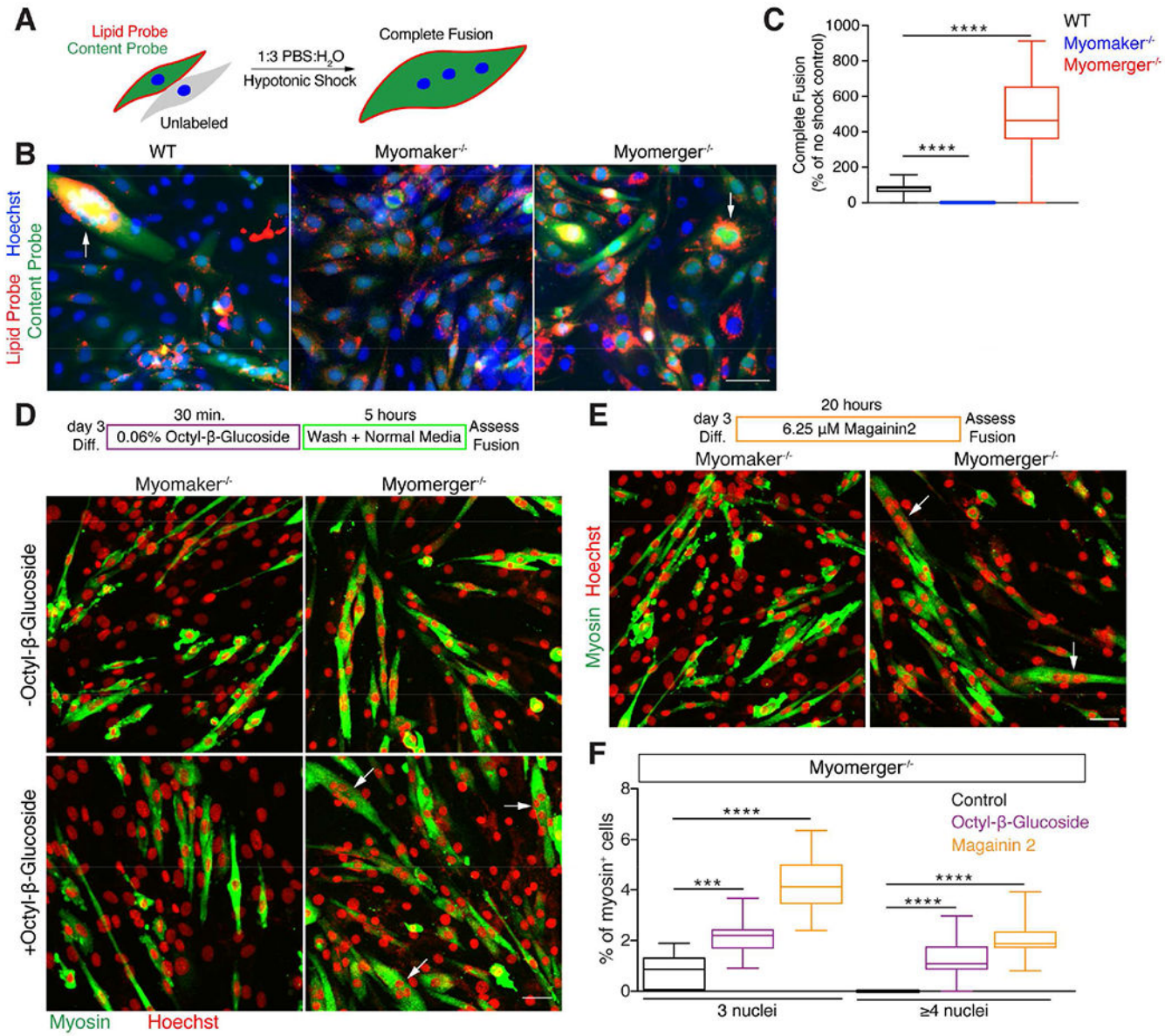

Figure 2. Compensation of Myomerger deficiency by heterologous membrane-stressing treatments.

(A) Schematic illustrating hypotonic shock fusion rescue experiment. Complete fusion is indicated by the presence of multinucleated cells labeled with both lipid and content probes. (B) Representative images of WT, Myomaker$^{-/-}$ and Myomerger$^{-/-}$ C2C12 cells differentiated for 48 hours, labeled with appropriate probes and plated in differentiation medium for 24 hours, then treated with PBS:H_2O (1:3) (hypotonic shock) for 60 seconds. (C) Quantification of complete fusion (n=3 independent experiments) as a percentage of cells of the same genotype that did not receive hypotonic shock. Myomerger$^{-/-}$ C2C12 myoblasts showed a significant increase in fusion when treated with hypotonic shock. (D) Treatment with Octyl-β-Glucoside (OG) on day 3 of differentiation (Diff.) induced fusion in Myomerger$^{-/-}$ myoblasts (arrows) but not in Myomaker$^{-/-}$ C2C12 myoblasts. (E) Treatment

with Magainin 2 (Mag2) for 20 hours on day 3 of differentiation induced myotube formation in Myomerger$^{-/-}$ C2C12 myoblasts (arrows) but had no effect on Myomaker$^{-/-}$ cells. For (D) and (E) the cells were immunostained with myosin antibodies to identify differentiated muscle cells and Hoechst dye was used as a nuclear stain. (F) The percentage of myosin+ cells that contain 3 or ≥4 nuclei after treatment with OG (n=3 independent experiments) or Mag2 (n=4 independent experiments) as an indicator of fusogenicity. Statistical analyses and data presentation: (C), (F), two tailed Student's t-test; box-and-whisker plots show median (center line), 25th–75th percentiles (box) and minimum and maximum values (whiskers); ***$P < 0.001$, ****$P < 0.0001$. Scale bars, 50 μm. See also Figure S2.

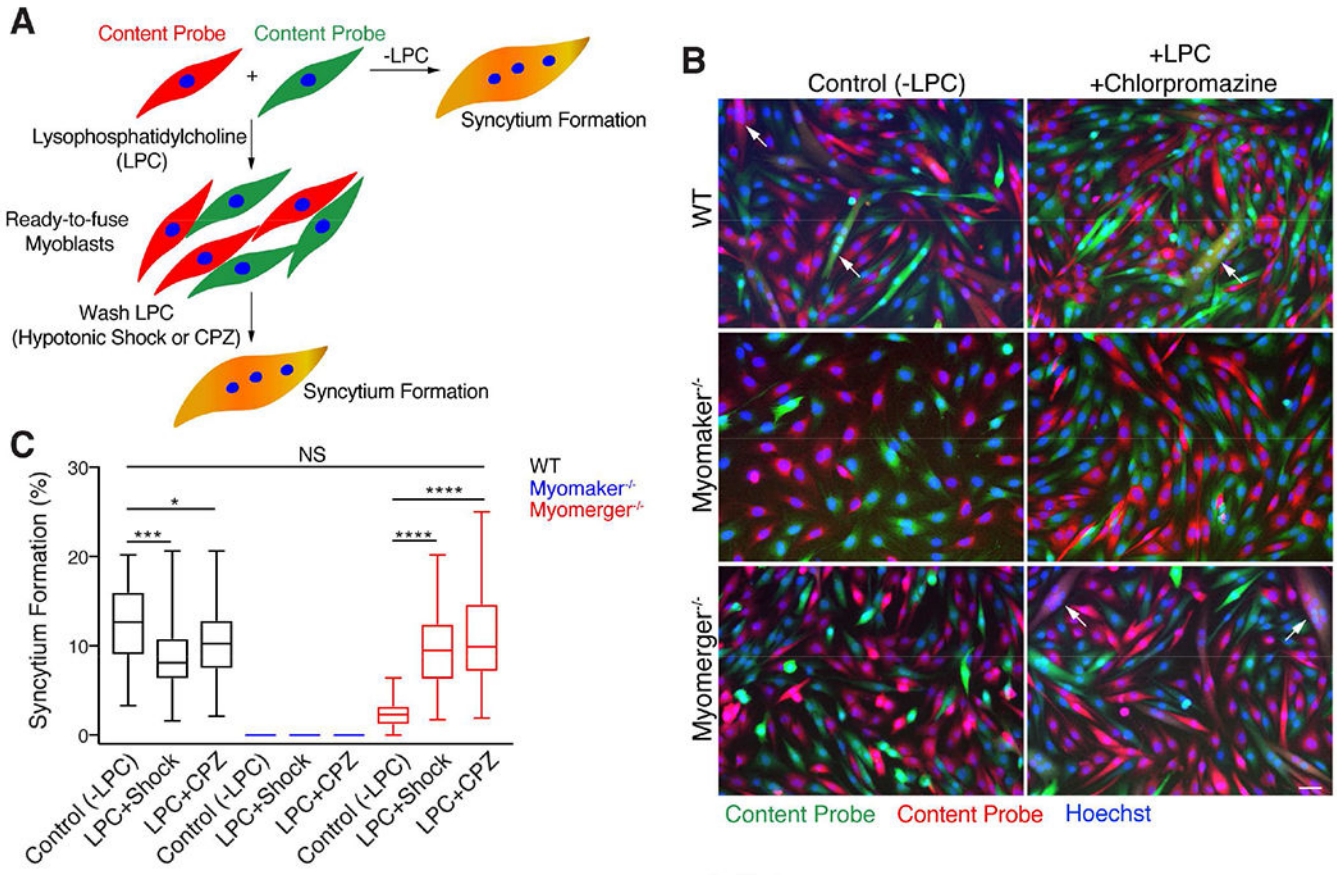

Figure 3. Myomaker does not require Myomerger to efficiently initiate hemifusion structures.

(A) Myoblasts were labeled with content probes (either orange cell tracker or green cell tracker) and differentiated for 48 hours. One set of myoblasts was allowed to fuse uninterrupted without LPC (Control (-LPC)), while others were treated with the synchronization agent LPC for 16 hours in differentiation medium to accumulate myoblasts that are ready-to-fuse. At the time of LPC removal, which allows cells to undergo hemifusion and complete fusion, the cells were exposed to either hypotonic shock (1:3 PBS:H_2O) or chlorpromazine (CPZ) for 60 seconds, washed and assayed for fusion after 30 minutes. (B) Representative images show fusion for myoblasts that were not exposed to LPC (Control (-LPC)) and myoblasts that were synchronized with LPC and then treated with CPZ. (C) Quantification of syncytium formation as the percentage of nuclei in multinucleated cells (defined as cells with 2 or more nuclei). Statistical analyses and data presentation: (C) Mann-Whitney test; box-and-whisker plots show median (center line), 25th–75th percentiles (box) and minimum and maximum values (whiskers); NS not significant, *$P < 0.05$, ***$P < 0.001$, ****$P < 0.0001$; Scale bar, 50 μm.

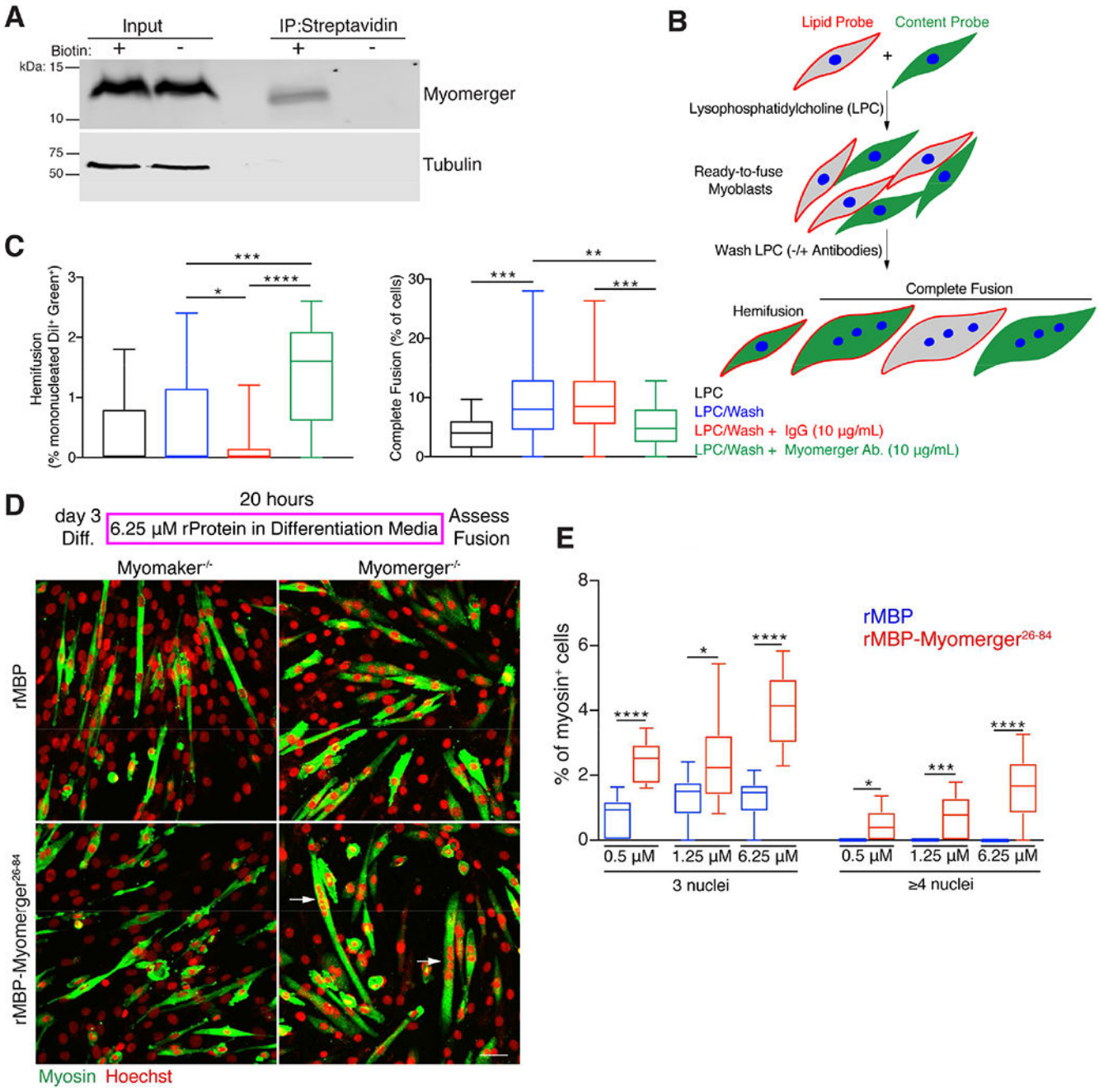

Figure 4. The C-terminal ectodomain of Myomerger functions from outside the cell.

(A) Immunoblot for Myomerger from the surface biotinylated fraction (IP: Streptavidin) and total lysates (input) from differentiated C2C12 myoblasts. Cells not treated with biotin were used as a control. Absence of the cytosolic protein (Tubulin) from the biotinylated fraction confirms surface-specific labeling. Data shown is representative from 3 independent experiments. (B) Schematic of the synchronized fusion assay. Myoblasts that had been differentiated for 48 hours were labeled with either DiI (lipid probe) or green cell tracker (content probe). Addition of LPC accumulates myoblasts that are ready-to-fuse and removal of LPC (LPC/Wash) allows cells to undergo hemifusion and complete fusion. Antibodies to

Myomerger ectodomain, or IgG as a control, were added during this wash phase. (C) Quantification of synchronized fusion for WT C2C12 (n=3 independent experiments) myoblasts was achieved by assessing formation of mononucleated cells with both membrane and content probes (hemifusion, left) and multinucleated myotubes (complete fusion, right). (D) Incubation of rMBP-Myomerger$^{26\text{-}84}$ for 20 hours in differentiation media induces fusion of Myomerger$^{-/-}$ (arrows), but not Myomaker$^{-/-}$ C2C12 myoblasts. Cultures were immunostained with myosin antibodies to identify differentiated muscle cells and Hoechst dye was used as a nuclear stain. (E) The percentage of myosin^{+} cells that contain 3 or ≥4 nuclei after incubation with rMBP or rMBP-Myomerger$^{26\text{-}84}$ (n=4 independent experiments with two independent protein purifications) at various concentrations of recombinant protein. Statistical analyses and data presentation: (C), (E), Mann-Whitney test; box-and-whisker plots show median (center line), 25th–75th percentiles (box) and minimum and maximum values (whiskers); *P < 0.05, **P < 0.01, ***P < 0.001, ****p < 0.0001; Scale bar, 50 μm. See also Figures S3, S4, and S5.

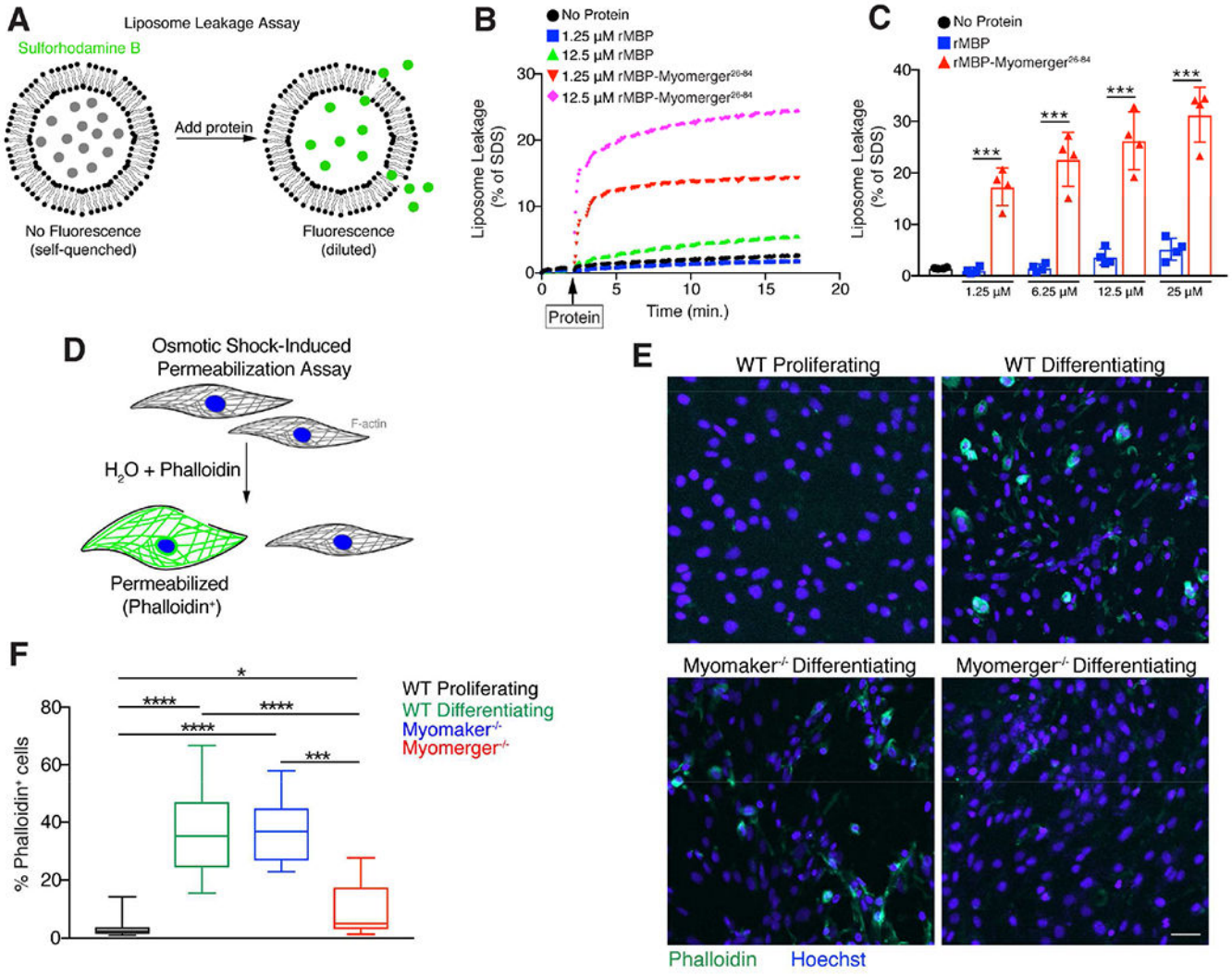

Figure 5. Myomerger functions to stress membranes.

(A) Schematic showing that disruption of the liposome membrane releases self-quenched Sulforhodamine B from the liposomes generating a fluorescence signal. (B) Liposome content release was monitored as an increase in Sulforhodamine B fluorescence and is presented as a percentage of the fluorescence measured after complete dequenching of the fluorescence by SDS application at the end of each experiment. Robust leakage was observed when liposomes were subjected to rMBP-Myomerger$^{26\text{-}84}$ but not to rMBP. (C) Analysis of leakage two minutes after the addition of various concentrations of recombinant protein (n=4 independent experiments with two independent protein purifications and two independent liposome preparations). (D) A permeabilization assay to determine an effect for Myomerger on the plasma membranes of cells. Myoblasts are incubated with water (induces osmotic swelling, membrane tension, and pore(s)) and fluorescent phalloidin (F-actin probe) for 30 seconds and detection of phalloidin^{+} cells indicates permeabilization. (E) Representative images show phalloidin labeling and Hoechst-labeled nuclei from proliferating WT C2C12 myoblasts and differentiating WT, Myomaker$^{-/-}$, and Myomerger $^{-/-}$ C2C12 myoblasts after hypotonic shock. (F) Quantification of the percentage of

phalloidin^{+} cells from E (n=3 independent experiments). Statistical analyses and data presentation: (C) two-tailed Student's *t*-test; (F) Mann-Whitney test; (C) mean ± standard deviation; (F) box-and-whisker plots show median (center line), 25th–75th percentiles (box) and minimum and maximum values (whiskers); *$P < 0.05$, **$P < 0.01$, ***$P < 0.001$, ****$p < 0.0001$; Scale bar, 50 μm. See also Figure S5.

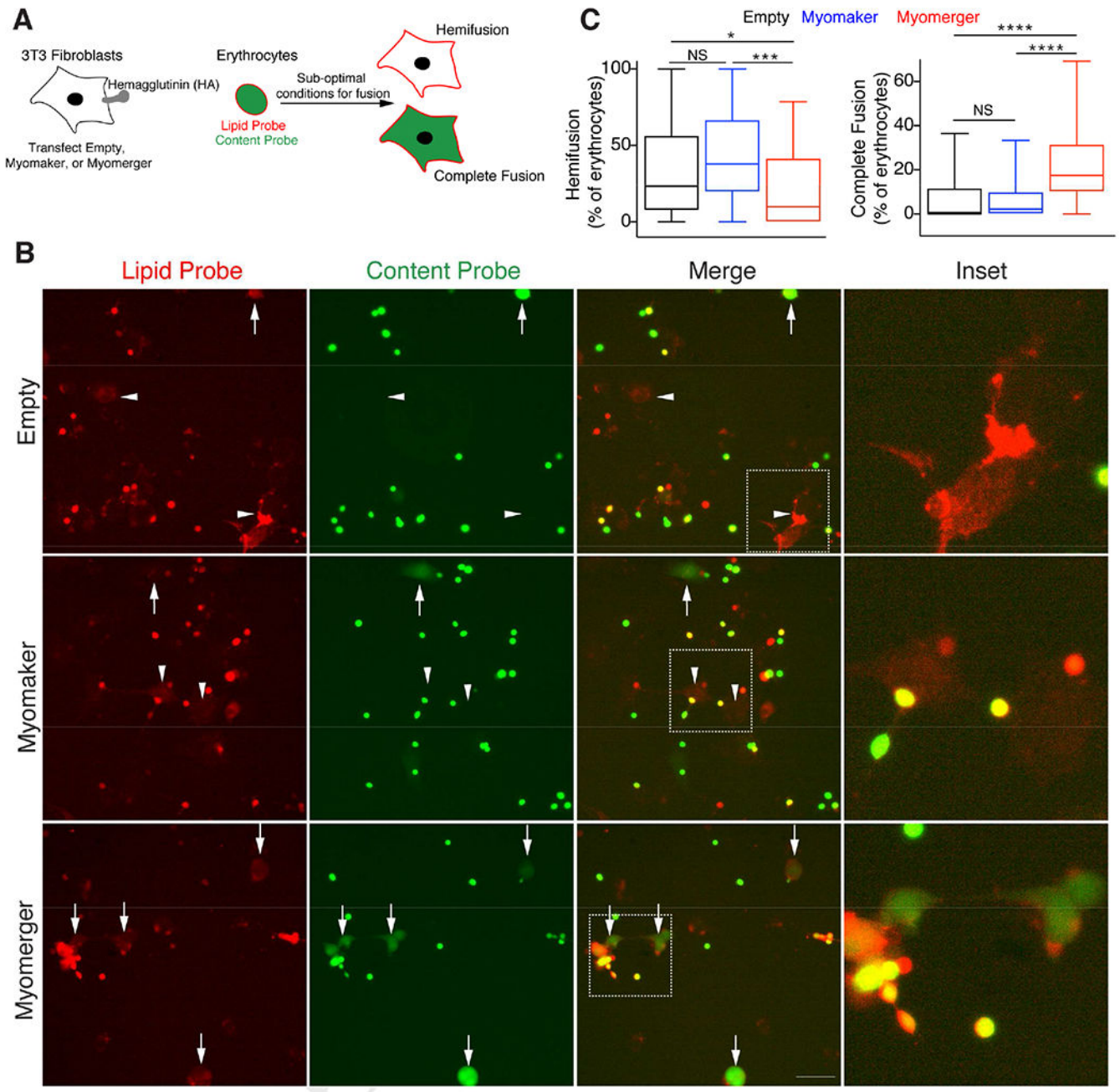

Figure 6. Myomerger drives fusion completion independent of Myomaker.

(A) Schematic showing heterologous fusion assay. 3T3 fibroblasts expressing hemagglutinin (HA) were transfected with empty, Myomaker or Myomerger plasmids and mixed with erythrocytes that were labeled with both lipid and content probes. (B) At selected sub-optimal conditions, HA only drives hemifusion (fibroblasts labeled with the lipid probe, arrowhead). Since fibroblasts are much larger than erythrocytes, hemifusion events are seen as appearance of large cells labeled with only lipid probe. Expression of Myomerger but not Myomaker drives complete fusion (fibroblasts labeled with both lipid and content probes, arrows). (C) Quantification of hemifusion (left) and complete fusion (right) from (B) (n=3

independent experiments). Statistical analyses and data presentation: Mann-Whitney test; box-and-whisker plots show median (center line), 25th–75th percentiles (box) and minimum and maximum values (whiskers); *$P < 0.05$, ***$P < 0.001$, ****$p < 0.0001$. NS, not significant. Scale bar, 50 μm. See also Figures S6 and S7.

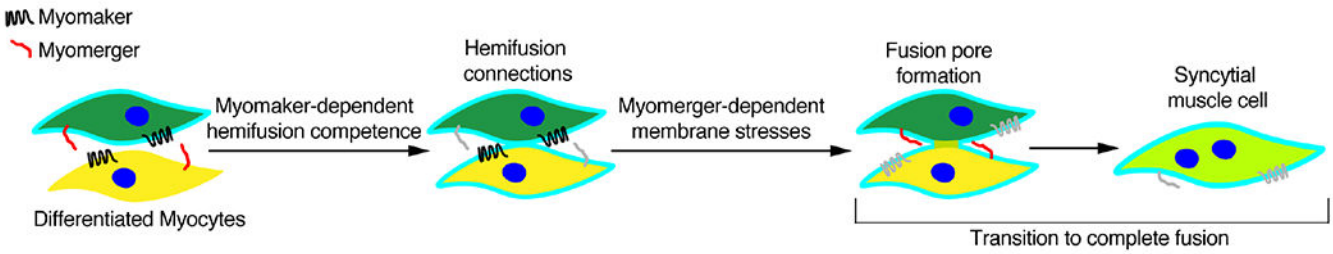

Figure 7. Schematic of the division of fusogenic labor between Myomaker and Myomerger.

Myomaker and Myomerger independently control two distinct stages of fusion in myoblasts. Both proteins are likely expressed simultaneously in differentiated fusion-committed myocytes. Colored proteins are shown during the stage at which they are essential although they may also be active during other times. At the first stage, Myomaker controls development of hemifusion competence and is indispensable for hemifusion connections (mixing of lipids (blue)), and Myomerger is not required for this step. The fusion reaction would stall at this stage without the presence of Myomerger, which at the second stage of the reaction generates membrane-stresses to drive the transition to complete fusion (green-yellow content mixing) in a Myomaker-independent manner. Note that the schematic is meant solely to illustrate how the independent activities of Myomaker and Myomerger cooperate during myoblast fusion, and the other factors that also impact the process are omitted for clarity.